fMRI-based effective connectivity in surgical remediable epilepsies: a pilot study

A.E. Vaudano[1,2], L. Mirandola[2], F. Talami[2], G. Giovannini[1,2], G. Monti[4], P. Riguzzi[3], L. Volpi[3], R. Michelucci[3], F. Bisulli[5,6], E. Pasini[3], P. Tinuper[5,6], L. Di Vito[5,6], G. Gessaroli[1], M. Malagoli[7], G. Pavesi[2,8], F. Cardinale[9], L. Tassi[9], L. Lemieux[10], S. Meletti[1,2].

[1]Neurology Unit, Azienda Ospedaliero-Universitaria of Modena, OCB Hospital, Modena, Italy
[2]Department of Biomedical, Metabolic, and Neural Sciences, Center for Neuroscience and Neurotechnology, University of Modena and Reggio Emilia, Modena, Italy
[3]IRCCS Istituto delle Scienze Neurologiche di Bologna, Unit of Neurology, Bellaria Hospital, Bologna, Italy
[4] Neurology Unit, AUSL Modena, Ospedale Ramazzini, Carpi Modena, Italy
[5] Department of Biomedical and NeuroMotor Sciences (DIBINEM), University of Bologna, Bologna, Italy
[6] IRCCS Istituto delle Scienze Neurologiche di Bologna, Epilepsy Center (Reference Center for Rare and Complex Epilepsies - EpiCARE), Bologna, Italy
[7]Neuroradiology Unit, Azienda Ospedaliero-Universitaria of Modena, OCB Hospital, Modena, Italy
[8] Neurosurgery Unit, Azienda Ospedaliero-Universitaria of Modena, OCB Hospital, Modena, Italy
[9] "Claudio Munari" Epilepsy Surgery Center, Niguarda Hospital, Milan, Italy.
[10] Department of Clinical and Experimental Epilepsy, UCL Queen Square Institute of Neurology, London, UK.

Running Title: *causal connectivity in surgical epilepsy*

Correspondence to:

Dr. Anna-Elisabetta Vaudano

Neurology Unit, OCB Hospital, AOU Modena,

Via Giardini 1355, 41100 Modena, Italy

Tel. +39059396170

Mail: annavaudano@gmail.com; annaelisabetta.vaudano@unimore.it;

Dr. Anna Elisabetta Vaudano ORCID 0000-0002-6280-7526

Dr. Francesca Talami ORCID 0000-0002-9245-4792

Dr. Giada Giovannini ORCID 0000-0002-3585-5872

Dr. Roberto Michelucci ORCID 0000-0002-9655-7940

Dr. Elena Pasini ORCID 0000-0001-6298-455X

Prof. Francesca Bisulli ORCID 0000-0002-1109-7296

Prof. Paolo Tinuper ORCID 0000-0002-0588-3063

Prof. Giacomo Pavesi ORCID 0000-0002-9004-1775

Dr. Francesco Cardinale ORCID 0000-0002-5141-9202

Dr. Laura Tassi ORCID 0000-0002-0632-7296

Prof. Louis Lemieux ORCID 0000-0003-3036-7412

Prof. Stefano Meletti ORCID 0000-0003-0334-539X

Abstract

Simultaneous EEG-fMRI can contribute to identify the epileptogenic zone (EZ) in focal epilepsies. However, fMRI maps related to Interictal Epileptiform Discharges (IED) commonly show multiple regions of signal change rather than focal ones. Dynamic causal modeling (DCM) can estimate effective connectivity, i.e. the causal effects exerted by one brain region over another, based on fMRI data. Here, we employed DCM on fMRI data in 10 focal epilepsy patients with multiple IED-related regions of BOLD signal change, to test whether this approach can help the localization process of EZ. For each subject, a family of competing deterministic, plausible DCM models were constructed using IED as autonomous input at each node, one at time. The DCM findings were compared to the presurgical evaluation results and classified as: "Concordant" if the node identified by DCM matches the presumed focus, "Discordant" if the node is distant from the presumed focus, or "Inconclusive" (no statistically significant result). Furthermore, patients who subsequently underwent intracranial EEG recordings or surgery were considered as having an independent validation of DCM results. The effective connectivity focus identified using DCM was Concordant in 7 patients, Discordant in two cases and Inconclusive in one. In four of the 6 patients operated, the DCM findings were validated. Notably, the two Discordant and Invalidated results were found in patients with poor surgical outcome. Our findings provide preliminary evidence to support the applicability of DCM on fMRI data to investigate the epileptic networks in focal epilepsy and, particularly, to identify the EZ in complex cases.

Keywords: "effective connectivity", "surgical epilepsies", "EEG-fMRI", "BOLD", "epileptogenic zone".

DECLARATIONS

Funding

Emilia-Romagna - SSN young researcher grant (project code GR-2013-02358466). SSN - RF grant: (project code NET-2013-02355313). Emilia- Romagna regional funding to the Azienda Ospedaliera-Universitaria di Modena “Centro hub chirurgia epilessia” (DGR 1172/18). Dipartimenti di eccellenza ‘2018-2022’, MIUR, Italy, to the Department of Biomedical, Metabolic and Neural Sciences.

Competing interests Statement

S. Meletti received research grant support from the Ministry of Health (MOH), the non-profit organization Foundation "Fondazione Cassa di Risparmio di Modena - FCRM"; he has received personal compensation as scientific advisory board member for UCB and EISAI. The other authors report no competing interests.

Data Availability Statement

The datasets that support the findings of the current study will be shared subject to limitations of the ethical approval of Area Vasta Emilia Nord Ethical Committee (http://www.aou.mo.it/ComitatoEticoAVEN)**.**

Ethical approval

This study was approved by the local Ethical Committee of Area Vasta Emilia Nord (N. 155/14) and written informed consent was obtained from all participants.

INTRODUCTION

Epilepsy occurs in 0.5-1% of people and about 25% of those affected continue to have seizures following the best medical therapies (Kalilani et al., 2018). Half of the patients with Drug Resistant Epilepsy (DRE) can benefit from epilepsy surgery, which is the most effective treatment, being successful in approximately 60% of cases (Liu et al., 2018). The precise localization of the Epileptogenic Zone (EZ), described as the driving hub of abnormal activity and seizures generation, organization and propagation, is crucial for a good surgical outcome (Duncan et al., 2016; Jehi, 2018). In contrast with a traditional focal model (the "zone" concept), a more dynamic concept of epileptogenic network has been progressively introduced, being defined as the set of the brain regions involved in the generation and propagation of epileptic activities (the "network" concept) (Bartolomei et al., 2017). According to the epileptogenic network view, post-operative seizure freedom might be improved by multitarget treatments alongside focal resection. This expanded concept of EZ opens the way to sophisticated non-invasive electrophysiological and neuroimaging methods that explore the epileptogenic network, its architecture and the relationships between its nodes. Ideally, these diagnostic techniques might help us understand the interplay between the epileptogenic tissue and the healthy brain in order to devise improved surgical strategies. However, despite advances, these approaches do not always reveal the smallest part of the cortex that require removal or disconnection, which remains the main clinical question for surgeons. The "zone" or "network" concepts of EZ are not necessarily mutually exclusive and need to be combined to achieve the best understanding of the individual EZ. Accordingly, while the epileptogenic zone is increasingly conceived as a network of nodes (sometimes even distant from each other) there is a big effort to identify the hierarchic involvement of its hubs and particularly to reveal the "leading" area/s in originating and sustaining seizures with respect to the "secondary" generators of synchronous activity. In patients with Focal Cortical Dysplasia (FCD), it was shown that within the stereo-EEG (SEEG) delineated epileptogenic network, advanced signal connectivity analyses identified the node which generates the pathological activity not only during the ictal events but also during the interictal period. In particular, this pattern

was distinguished from the other cortical regions involved by ictal/interictal activity, thus clearly recognized as secondary “hubs” (Varotto et al., 2012).

In clinical practice, DRE patients may undergo long-term electroencephalograph, functional imaging (fMRI, PET, ictal SPECT, MRS, or MEG) and neuropsychological testing aimed at localizing the EZ as part of a presurgical workup (Brodbeck et al., 2011; Markoula et al., 2018; Rampp et al., 2019; Duez et al., 2019). In cases in which such data are unsatisfactory, further, invasive investigations in the form of intracranial EEG recording: (icEEG) (which may be considered the “gold standard” for the EZ localization) may be performed (Vakharia et al., 2018). However, this approach is best warranted based on a solid hypothesis about the location of the epileptogenic network provided by the results of previous tests, due to the spatial sampling limitations, health risks and costs associated with icEEG (Khoo et al., 2017; Vakharia et al., 2018; Cardinale et al., 2019). Therefore, there is a need for the development of alternative and/or complementary non-invasive image techniques to improve the localization of the EZ, and to characterize the architecture of the epileptic network.

Simultaneous scalp EEG-fMRI is a technique capable of revealing brain regions associated with interictal epileptic discharges (IED) based on local blood oxygen level-dependent (BOLD) signal variations (Khoo et al., 2017; Pittau et al., 2012; Thornton et al., 2011). In surgical epilepsy, this technique has attracted interest as a preoperative diagnostic tool to localize the EZ non-invasively (Gotman & Pittau, 2011). Recently, an observational prospective cohort study showed that IED-related fMRI findings can affect the clinical decision making and patients’ management process in a substantial proportion of DRE cases investigated as part of their presurgical evaluation (Markoula et al., 2018). Additionally, EEG-fMRI was shown to influence directly the decision to offer surgery in patients with focal epilepsy (Kowalczyk et al., 2020). Regions of IED-related BOLD change provide useful localization information on the irritative zone, which is defined as the area of the cortex generating IED (Jehi, 2018; Zijlmans et al., 2019), and which might be widespread or larger than the required resection area in focal epilepsy. For this reason its role as a marker of the EZ is debated (Lüders et al., 2006). Nevertheless, it has been demonstrated that in many cases the regions of IED-

related BOLD change are a good predictor of the seizure-onset-zone (SOZ) as revealed by icEEG and/or the surgery clinical outcome (Thornton et al., 2011; Pittau et al., 2012; An et al., 2013; Coan et al., 2016; Khoo et al., 2017). Additionally, a good concordance was reported between interictal BOLD changes and ictal data (Tyvaert et al., 2008). Recently, an excellent correspondence between the region of maximum BOLD change correlated with IEDs on scalp EEG and the icEEG-defined seizure onset zone has been shown (Khoo et al., 2017, 2018), with an accuracy of more that 90% in some situations (Khoo et al., 2017). Compared to other not-invasive presurgical techniques, the presurgical IED-related EEG-fMRI shows higher specificity to identify the EZ particularly in patients with MRI negative focal epilepsy and suspected extended EZ (Rossi Sebastiano et al., 2020). However, despite encouraging results, the sensitivity and reliability of IED mapping using EEG-fMRI remains limited (Yamazoe et al., 2019). Previous EEG-fMRI studies reported that BOLD changes were able to identify accurately the EZ in a variable proportion raging between 53-88% of focal epilepsy patients (Pittau et al., 2012; Coan et al., 2016; Khoo et al., 2017). This high variability is thought to be related to three main factors: (*a*) the heterogeneity of clinical epilepsy syndromes and cohort's size; (*b*) differences in EEG and fMRI analysis pipelines; and (*c*) the definition of BOLD concordance criteria with other non-invasive and/or invasive investigations to establish the clinical relevance of the fMRI clusters' localization. While in some studies, the IED-related BOLD clusters were defined as "*concordant*" if the cluster with maximum *t*-value corresponded to the localization of the spike-field determined by scalp EEG (Pittau et al., 2012, 2017), others assessed the concordance on the primary fMRI clusters by estimating the proximity (usually within 2 cm) with the EZ as revealed by icEEG recordings (Khoo et al., 2017; Thornton et al., 2011) or the area of surgical resection (An et al., 2013; Coan et al., 2016). A common observation is that focal IED-related BOLD maps comprise two or more clusters of activations or deactivations, distributed over multiple lobes (An et al., 2013; Coan et al., 2016; Thornton et al., 2011). Furthermore, it has also been shown that the whole of any given IED-related BOLD map can contain clinically-relevant information, with a degree of predictive power for the outcome of patients who subsequently underwent surgery; for

example, maps with multi-lobar activations and deactivations are associated with poorer surgical prospects (An et al., 2013; Coan et al., 2016; Khoo et al., 2017; Thornton et al., 2011). Therefore, if the aim is to better identify the EZ, there is a need for more investigations on the clinical relevance of the multiple clusters that constitute many IED-related BOLD maps. In particular, we need to better understand the dynamics that underlie these BOLD maps, seen as networks, and more specifically, the possibility of identifying the brain regions that act as 'sources' of the activity in the rest of the network.

Dynamic Causal Modelling (DCM) is an analysis framework for the characterization of brain effective connectivity i.e., the causal interactions between neuronal systems (Friston et al., 2003) and hence can potentially be used to identify the neuronal drivers of pathological activity. DCM applied to fMRI allows to establish the causal influences between the activities in a set of brain regions, despite the limitation of temporal resolution inherent to this imaging technique. DCM for fMRI data, in addition to its application to task-based paradigms, has been applied to resting-state data from patients affected by generalized and focal epilepsies (Vaudano et al., 2009, 2012, 2013; Murta et al., 2012; Klamer et al., 2015, 2018; Warren et al., 2019), to identify the sources ('drivers') of the pathological activity and/or the causal connectivity between epilepsy-related BOLD clusters. Up to now, only a few single-case reports used this methodology in surgically-remediable epilepsies (Vaudano et al., 2013; Klamer et al., 2015).

In the following, we present the results of the use of DCM on fMRI data acquired during rest to help localize the EZ in a group of consecutive patients with focal epilepsy who were candidates for surgery and in whom multiple IED-related BOLD clusters were revealed by analysis of the concurrently recorded EEG-fMRI.

DATA and METHODS

2.1 Study population

From an original pool of 35 patients with surgically remediable epilepsies who consecutively underwent EEG-fMRI for mapping of their inter-ictal epileptiform activity (IED) from January 2013 to December 2017, we selected all the adult patients (≥18 years old) who presented IED-related fMRI maps with multiple clusters, including at least one (either activation or deactivation) co-localized with the presumed EZ based on the result of the not-invasive pre-surgical work-up. The patients were collected from the two Epilepsy clinics that form the Epilepsy Surgery hub of the Emilia-Romagna Region (Italy): the Azienda Ospedaliera-Universitaria di Modena, in Modena, Italy and the IRCCS Istituto Scienze Neurologiche, AUSL Bologna, Italy. Both centers were in charge to perform the presurgical work-up. The EEG-fMRI studies were acquired and analyzed in Modena. This study was approved by the local Ethical Committee of Area Vasta Emilia Nord (N. 155/14) and written informed consent was obtained from all participants.

2.2 MRI and EEG-fMRI acquisition, processing and analysis

The following structural MRI data were acquired using a 3T MRI scanner (Philips Intera): a high-resolution 3D T1-weighted anatomical MR image (3D-T1) was acquired consisting of 170 sagittal slices (TR = 9.9 ms; TE = 4.6 ms; voxel size = 1 mm^3); A high-resolution 3D fluid-attenuated inversion recovery (FLAIR) (TR = 4.8 ms; TE = 3.1 ms; voxel size = 1.2x1.2x1.2 mm^3). In addition, for patients who subsequently underwent resective surgery, postsurgical 3D-T1 MRI were acquired at 6 and 12 months after surgery.

Scalp EEG was recorded by means of a 32-channel MRI-compatible EEG recording system (Micromed, Italy) concurrently with fMRI. The fMRI data was acquired using a gradient-echo echo-planar imaging sequence (EPI) sequence from 30 axial contiguous slices (TR = 2.000 ms; voxel size: 3.75 × 3.75 × 4 mm) over one or two fMRI runs (240 volumes/run, 8 minutes each run) with

continuous simultaneous EEG recording. Patients were asked to remain still during the scanning with eyes closed and do not fall asleep.

After offline correction for the scanner gradient artifacts and filtering of the EEG signal, the EEG data were reviewed and preprocessed according to a previous published method (Avanzini et al., 2014). Two experienced electroencephalographers (AEV, LM) reviewed the EEG recordings independently to identify the IED. IED definition follows specific morphological and topographic criteria as recently updated by the International Federation of Clinical Neurophysiology (Kane et al., 2017). Additionally, only IED similar to those recorded outside the scanner were marked, resulting in a set of IED event time markers, and durations for the interictal events that consist of runs of spike-wave discharges. In some recordings, with more than one type of IED, each event was labelled according to its type. The similarity between the IED recorded inside and outside the scanner was verified visually and by analyzing the scalp topographic map. To this end, the marked spikes were averaged, and the voltage map estimated and compared to the interictal spike field observed during the clinical video-EEG monitoring. Indeed, among the established criteria to define IED, one of the best performing is represented by the inspection of the voltage topography (Kural et al., 2020).

The Matlab 15.1 and SPM12 (Wellcome Centre for Human Neuroimaging, UCL, London, UK) software were used for fMRI data analysis. Preprocessing steps consisted of: (*a*) slice timing correction to account of the interleaved acquisition; (*b*) motion correction; (*c*) co-registration of the 3D-T1 scan to the mean EPI fMRI; and (*d*) spatial smoothing with a 8-mm full-width-at-half-maximum Gaussian kernel. The six motion parameters derived from the fMRI preprocessing (translation and rotation in the X, Y, and Z direction, respectively) and a Volterra expansion of these (Friston et al., 1996) were used as covariates in the general linear model (GLM). The effects of interest consisted of the IED, each represented as either a stick function or variable-duration block, were convolved with the standard hemodynamic response function (HRF) and its temporal and dispersion derivatives (Lemieux et al., 2008; Hamandi et al., 2006; Salek-Haddadi et al., 2006). In recordings in which multiple IED types were identified, each type was included as a separate effect

of interest in the GLM. The resulted fMRI maps (F-contrast) were estimated at conventional statistical threshold of $p<0.05$ (family wise error (FWE)-corrected). In addition, in cases where conventional FWE corrected statistical threshold did not show any results, the data were further explored with a less stringent statistical threshold of $p<0.001$ (uncorrected for multiple comparisons). In the latter case, we applied a small volume correction (5 mm sphere) and we considered any BOLD activation/deactivation with a cluster-level threshold at $p < 0.05$, FWE corrected. This multiple-levels statistical approach is in line with previous similar studies (Poldrack, 2007; Chaudhary et al., 2012; Coan et al., 2016; Markoula et al., 2018; Rossi Sebastiano et al., 2020).

2.3 Identification of the presumed EZ

The presumed EZ (pEZ) was defined based on the results of the presurgical work-up, which included: ictal clinical semiology, scalp EEG interictal spike field (i.e. the region thought to generate the IED), scalp EEG ictal activity, structural MRI scan, and interictal F-18 fluorodeoxyglucose FDG-PET when available. For each patient, the spike field was estimated at sub-lobar level by visual inspection. This information was discussed together with the other clinical and neuroradiological findings at a multidisciplinary team meeting resulting in a consensus EZ localization. The results of the EEG-fMRI analysis were not considered in the clinical evaluation or EZ localization process.

2.4 IED-related BOLD map concordance with pEZ

In order to inspect the spatial relationship between the map of IED-related BOLD changes and the pEZ, as defined previously, we adopted the following pipeline for each patient:

1. The high-resolution anatomical 3D-T1 MRI scan underwent cortical and subcortical segmentation using a standardized image toolbox (*Freesurfer*, version 6.0), following standardized ENIGMA protocols for image quality check (Whelan et al., 2018). The resulting cortical and subcortical parcellation was used for anatomical labelling.

2. The FLAIR, mean EPI, PET datasets were linearly registered to the high-resolution 3D-T1 MRI using FMRIB Software Library (FSL) (www.fmrib.ox.ac.uk/fsl/fslwiki/flirt) (six-parameter rigid-body transformation).
3. The F-map was then coregistered to the anatomical 3D-T1 MRI using the co-registration matrix derived from the registration of mean-EPI to the T1-weighted image.
4. The resulting co-registered EEG-fMRI, anatomical and PET data were visualized using the 3D Slicer software (Fedorov et al., 2012) or *Freeview* toolbox (https://surfer.nmr.mgh.harvard.edu/fswiki) and inspected for correct alignment and co-registration (AEV, FC).

The level of concordance/discordance between the BOLD map and the EZ was defined based on previous published criteria (Rachel Thornton et al., 2011; Chaudhary et al., 2012; Markoula et al., 2018). Specifically, 'Concordant' (*C*) refers to maps in which all the clusters (either activation or deactivation) colocalized with the pEZ: within 2cm of and in the same lobe as EZ; 'Concordant Plus' (*C*+) is applied to fMRI maps with some clusters of significant IED-related BOLD changes colocalized with the pEZ and other significant BOLD clusters were located within the same lobe or touching the edge of the same lobe as the pEZ; Discordant Plus (*D*+) refers to the situation where some clusters of significant IED-related BOLD changes were localized within the pEZ, with other significant BOLD clusters in other lobes; Discordant (*D*) where all clusters of IED-related BOLD changes were remote from the pEZ and Null (*N*) where there was no cluster of significant IED-related BOLD change.

For the purpose of the present study only EEG-fMRI maps labelled as *C*+ and *D*+ were further analyzed using the DCM approach. This will allow us to evaluate the results against the independently determined pEZ as part of this proof of concept study. The *C*, *D* and *N* maps were excluded from the DCM analysis: the *C* maps consisted of clusters co-localized with the pEZ exclusively, while the *D* and *N* maps did not include any clusters co-localized with the pEZ.

2.6 Effective connectivity analysis and interpretation

For each EEG-fMRI *C+* and *D+* map, DCM was used to compare competing models of the causal connectivity between the IED-related BOLD clusters. Specifically, we aimed to identify the 'source' of the recorded epileptic activity, modelled as a causal driver, in contrast to the nodes that are thought to be part of propagation pathways.

DCM analyses were performed with the DCM10 module in SPM12, with models parameterized using the bilinear differential equation for fMRI in DCM (Kahan & Foltynie, 2013; Friston et al., 2003). For each EEG-fMRI dataset, we devised a series of competing models clinically meaningful based on the available electro-clinical information (clinical, EEG, neuroimaging), as follows:

First, a region-of-interest (ROI) (5 mm radius) was defined within the significant activation/deactivation clusters revealed by the SPM{F} contrast. The sign of the BOLD change for each cluster was determined by plotting the fitted response at the most significant voxel within the cluster. An examination of the IED-related BOLD maps was performed to identify the clusters that are candidate for EZ, and all deactivations in the Default Mode Network (DMN) were excluded as they usually do not represent realistic generator of IED. To define the DMN deactivations, the maps were first inspected visually then were labelled with BrainMap70 Atlas (Ray et al., 2013) using the ICN_Atlas tool (Kozák et al., 2017).

Second, for each selected ROI, the time series was extracted using the principal eigenvariate at the voxels surviving a threshold of $p< 0.01$ (uncorrected) or $p<0.05$ (corrected), and adjusted using the {*F*} contrast of effects of interest.

Third, a family of dynamic causal models were devised consisting of all the ROIs, fully intrinsically connected (backward and forward; DCM matrix *A*), and with bilinear effects in the form of the modulation of connection strength (matrix *B* in DCM) by the IED onsets/durations considered as the driving input (DCM matrix *C*) at one of the ROI's, taking each in turn. Thus, each model represents a different hypothesis concerning the driving input ('driver') that is hypothesized to perturb the neuronal activity and thereby, cause the observed IED-related BOLD changes.

Fixed Effect (FFX) Bayesian Model Selection (BMS) was used to compare the models at the subject level. Each model's Free Energy, *F*, a lower bound of the model's log-evidence, accounting for model complexity as well as data fit, was used to compare the likelihood of the different models to explain the data. Relative log-evidences, or differences in *F*, were converted into model posterior probabilities, *p*, indicating that the respective model has a probability *p* of being the best model/family explaining the data amongst all considered. Evidence was "strong" if $p>0.95$ (which corresponds to a difference in *F* greater than 3), and "positive" if $0.75<p<0.95$, which stands for a difference of *F* between 1 and 3 (Penny et al., 2004). In the latter situation, DCM findings were classified as "*inconclusive*", as they did not end up with significant results (i.e. there is no single winning model). For the cases with a conclusive DCM result, this was validated against the pEZ. DCM findings were labelled as "*Concordant*" if the driver identified by the connectivity approach corresponds to the pEZ as previously defined and "*Discordant*" otherwise.

2.7 Independent validation of DCM findings

For the patients who subsequently underwent SEEG or resective surgery a "two-step" independent validation process of the DCM findings was applied, as follows: in the first step, the winning DCM model was considered *validated* if the revealed source includes the contacts recording from the SOZ as revealed by visual SEEG inspection (Cardinale et al., 2019) or was comprised in the surgical resection area, and *invalidated* otherwise. For this purpose, the fMRI maps were visualized in relation to the SEEG electrodes position or the resection area, by co-registering the post-implantation images [(computed tomography [CT]) (for subjects who underwent SEEG) and the postsurgical 3D-T1 MRI] and the pre-implantation anatomical 3D-T1 MRI by means of a rigid-body transformation using FSL (https://fsl.fmrib.ox.ac.uk/fsl/fslwiki/FLIRT). The positions of the SEEG recording contacts were automatically estimated using SEEGA (Narizzano et al., 2017).

In the second step, the DCM result from each surgical patient was classified as confirmed or unconfirmed in consideration of the post-surgical outcome, based on the principle that a bad outcome

reflects inadequate characterization of the SOZ, thus undermining the confirmation of any localization result. Outcome was defined as good for Engel's classes I-II and poor for classes III-IV at one year (Engel, 1993).

Therefore, the possible outcomes of the two-step validation of DCM result for each patient are four-fold: (a) "*SEEG/surgery-validated and confirmed*" if the DCM findings was concordant with SEEG/surgery and surgical outcome was good; (b) "*SEEG/surgery-validated but unconfirmed*" if the DCM result was concordant with SEEG/surgery but surgical outcome was poor; (c) "*SEEG/surgery-invalidated but unconfirmed*" if the DCM result was discordant with SEEG/surgery and surgical outcome was poor; (d) "*SEEG/surgery-invalidated and confirmed*" if the DCM result was discordant with SEEG/surgery but the surgical outcome was good.

3. RESULTS

3.1 Electro-clinical and EEG-fMRI characteristics

10 out of 35 patients (28%) [5 male, mean age 29.1 (SD: ± 9.2), mean epilepsy duration 13.9 years (SD±8.6)], with multiple clusters of IED-related BOLD changes as described above underwent the DCM effective connectivity analysis. See the **Supplementary Figure S1** for a schematic representation of the EEG-fMRI findings of the entire population. Five out of 10 patients were affected by Temporal Lobe Epilepsy (TLE), 3 by Parietal Lobe Epilepsy (PLE) and 2 patients by Frontal Lobe Epilepsy (FLE). Only one patient had a normal structural MRI scan; 9 patients had a structural lesion on the MRI scan [Focal Cortical Dysplasia (FCD) in 5, perysilvian polymicrogyria in 1, Dysembryoplastic Neuroepithelial Tumors (DNET) in 1, arteriovenous malformation (AVM) in 1 and dermoid cyst in the remaining]. 6/10 patients underwent surgery with a mean follow-up of 32.8 ± 20.7 months (range 12-72), two of which (Patients #2,3) underwent SEEG prior to surgery. Surgical outcome was classified as Engel Class I in 3 patients (Patients #2,3,4), II in one (Patient #8), III in the remaining two cases (Patients #7,10). Detailed electroclinical information is provided in **Table 1**. 5/10 IED-related BOLD maps consisted of 2 clusters, 3/10 had three clusters and the remainder had 4 clusters (**Table 2**). The cluster containing the global statistical maximum matched the pEZ in 3/10 cases while for the other patients, smaller secondary clusters matched the pEZ. Four patients were labelled as *C+*, two of them were affected by FLE (Patients #1,6) and two by TLE (Patients #4,9); patient #4 underwent surgery. The remaining 6 cases were labelled ad *D+*: 3 had TLE (Patients #2,5,10) and 3 PLE (Patients #3,7,8), and five underwent surgery (Patients #2,3,7,8,10).

3.2 Effective connectivity driver identification

In relation to the pEZ, the effective connectivity driver identified using DCM model comparison was *Concordant* in 7 patients (70%; Patients #1,2,3,4,5,6,8), *Discordant* in two cases (20%; Patients #7,10) and *Inconclusive* in one (10%; Patient #9) (**Table 2)**. Among the concordant results, 2 patients were affected by FLE due to structural lesions, 3 patients by TLE (2 cases due to FCD, one subject with cryptogenic epilepsy) and 2 by PLE due to polymicrogyria and FCD respectively. The two

discordant findings were both cases with focal symptomatic epilepsy: one patient with parietal FCD and one patient with temporal vascular malformation. The inconclusive result concerns a patient with a temporal mesial DNET (**Figure 1**). Independent validation of DCM findings was obtained in 6 patients (60%) by surgery and in two of them by surgery and SEEG (Patients #2,3). In 4 out of 6 patients (66%), DCM findings were *surgery-validated* (Patients #2,3,4,8), *surgery-invalidated* in two (33%) (Patients #7,10). Considering the post-surgical outcome, all the *validated* DCM findings were *confirmed* (good outcome), while the two *invalidated* results were classified *unconfirmed* as the clinical outcome after surgery was poor (Engel Class III) (**Table 2**). **Figure 2** describes a representative case of *concordant, SEEG/surgery-validated* and *confirmed* DCM result, **Figure 3** a patient with *discordant*, *surgery-invalidated* and *unconfirmed* DCM result and **Figure 4** refers to the patient with an *Inconclusive* DCM result. For all the other patients, see **Supplementary Figures S2-S8.** See **Table S1** for the details of the DCM model comparisons.

4. DISCUSSION

This "proof of concept" work represents the first attempt to investigate the possibility of identifying putative drivers of human focal epileptic activity using DCM on fMRI data. In order to assess the method's potential, we focused specifically on patients with surgically remediable epilepsy whose IED-related EEG-fMRI maps show widespread/multiple activations with at least one concordant with pEZ in order to elucidate the generators of interictal epileptiform discharges within the network. By comparing small sets of models of effective connectivity derived from the BOLD maps we found that the method has the capability to identify unique drivers located within the presumed epileptogenic zone in a large proportion of cases.

DCM applied to fMRI data has been used successfully to investigate the effective connectivity within the epileptic networks in patients affected by generalized epilepsies (Vaudano et al., 2009; Klamer et al., 2018) and reflex epilepsies (Vaudano et al., 2012) at the group and single-subject levels. In these contexts, DCM was used to infer the causal relationship between various BOLD clusters, adding significant knowledge on the pathophysiological circuitries behind these "system epilepsy" conditions (Avanzini et al., 2012). In potentially surgically remediable focal epilepsy, where the main clinical question is that of identifying the focus or origin of epileptic activity, the application of this methodology is even more appealing for diagnostic purposes, due to the lack of success of the EEG-fMRI approach to reveal the EZ in a large proportion of patients (Kowalczyk et al., 2020; Yamazoe et al., 2019). Nevertheless, up to date, knowledge on the technique's clinical relevance is limited due to the small number of cases studied (Hamandi et al., 2007; Murta et al., 2012; Vaudano et al., 2013; Klamer et al., 2015). To attempt to address this, we used DCM on IED-related fMRI maps in 10 consecutive focal epilepsy patients to investigate whether it can contribute to the localization of the EZ. Overall, our findings support the contention that DCM applied to interictal fMRI maps might contribute to identify the EZ in patients with multiple IED-related hemodynamic clusters, thus adding value to EEG-fMRI as part of epilepsy presurgical protocols.

4.1 Widespread IED-related BOLD Maps in Focal Epilepsies

Previous studies have shown that fMRI mapping of IED on scalp EEG are of localizing value and predictive value for post-surgical outcome (An et al., 2013; Kowalczyk, et al., 2020; Markoula et al., 2018), with a concordance with the presumed EZ in up to 88% of patients (Pittau et al., 2012). However, in most studies the pool of patients with "concordance" between IED-related BOLD responses and the EZ included cases with concordant plus/discordant plus maps: i.e. with multiple clusters, including at least one co-localized with the EZ. In this work, out of a pool of 35 patients, nearly one/third (10/35, 28%) demonstrated multiple widespread IED-related BOLD clusters involving either the same hemisphere of EZ (*C+*, 40%) or the contralateral (*D+*, 60%), in line with previous reports (Thornton et al., 2011; Markoula et al., 2018). The common observation of multiple or widespread IED-related EEG-fMRI maps support the notion that this tool is perfectly suited to image the epileptic network. It has been shown that IED-related EEG-fMRI is able to identify clusters of signal increase concordant with the spike onset zone [i.e. a region where a spike is initiated, (Khoo et al., 2018)] and the regions where the spike propagate (Watanabe et al., 2017) which might be remote from the IED generator. This good performance of EEG-fMRI has been demonstrated even in cases of deep IED sources such as in patients with mesial TLE (Yamazoe et al., 2019) and in patients with cortical malformations (Pittau et al., 2017; Thornton et al., 2011), where multiple areas of epileptogenicity can be observed. In the contest of epilepsy surgery, where the identification of the epileptic focus is required, however, these complex maps need deeper understanding to highlight the clinical relevance of each node within the revealed network and specifically to identify the generator/s of IED as often corresponding to the EZ. It has been observed that the IED-related BOLD cluster containing the voxel with highest statistical score, named "primary cluster" or "global maxima", often has the highest localizing value with respect to the SOZ as delineated by intracranial EEG (Khoo et al., 2017). Additionally, in cases of widespread IED recorded intracranially, it has been shown that the IED recorded close to the maximum hemodynamic response are more likely to precede those recorded remotely, and that the IED delay in a particular channel is correlated with the distance

between its location and the maximum hemodynamic response (Khoo et al., 2018). In our cohort, the global statistical maximum was concordant with the presumed EZ in only 3 out of 10 patients Patients #6,7 and 9). The discrepancy between our findings and previous evidences could be due partly to methodological differences. Herein, we adopted an {*F*} contrast to evaluate fMRI maps as best fits data in our model with canonical HRF and derivatives whereas others estimated the global maximum based on the maximum *t* values (Khoo et al., 2017). Furthermore, the findings in some of the patients studied here might reflect complex epileptic circuits as observed in patients with multifocal epilepsy or unknown epileptic focus (Thornton et al., 2011; González Otárula et al., 2018). Indeed, in such circumstances, it was shown that secondary clusters rather than the primary one might be consistent with the highest high-frequency-oscillation (HFO) rates recorded by SEEG (González Otárula et al., 2018). In our population however, even in highly focal cases (Patients#1, 4 and 8) in whom the totality of not-invasive investigations points toward a clear focus, the global maximum was discordant. Although we are aware that some of these patients are waiting for surgery and the sample is small to draw conclusions, our findings suggest the importance of consider even so-called 'secondary' BOLD clusters as they might of help in identifying the epileptogenic regions in focal epilepsies.

4.2 Dynamic Causal Modelling

We hypothesized that DCM applied to IED-related BOLD maps can be a useful approach to infer the effective connectivity between the nodes of the epileptic networks. This is potentially highly relevant in the contest of epilepsy surgery when the IED-related BOLD maps show multiple clusters of hemodynamic changes and given the inconclusive sensitivity of the global maximum to reveal the epileptogenic focus.

Generally speaking, the effective connectivity corresponds to the directed ("causal") influence that one region exerts on the activity in another, in other words: it can be used to test which brain region drives which (Kahan & Foltynie, 2013). Compared to previous classical models of effective connectivity for fMRI data (like psycho-physiological interactions (PPI), or structural equation

modeling (SEM)), DCM combines a neurobiologically plausible model of neural dynamics with biophysically plausible hemodynamic model that describes the transformation of neuronal activity into a BOLD response (Stephan & Friston, 2010). Both sets of parameters describing the neuronal and the forward model of BOLD signal generation are estimated from each brain region included in the model using a Bayesian framework (Penny et al., 2004). This approach aims to refine the model parameters in order to produce a predicted signal that is close as possible to the observed BOLD data (Stephan & Friston, 2010). In the neuronal model in DCM for fMRI data, like the approach used here, propagation delays are not modeled because fMRI data does not contain enough temporal information due to considerable inter-regional variability in hemodynamic response latencies (Kahan & Foltynie, 2013). Instead, the differential latencies of the hemodynamic response are accommodated by region-specific biophysical parameters in the hemodynamic model. Nevertheless, causality in DCM does not only rely on temporal precedence but takes into account when and where the system is perturbed by external or endogenous brain influences and the structural connectivity within the system (Friston et al., 2003; Stephan & Friston, 2010). Herein, we presumed the interictal EEG activity as an extrinsic input which perturbs the investigated network. The time of IED onset is thus conceived to be the initial cause of the modeled effects as it can influence directly the neuronal states of the specified anatomical nodes. This assumption might be of concern due to such an endogenous type of activity. In addition, the IED onset as recorded from the scalp might be delayed with respect to the real interictal activity onset and represent only a fraction of what really happening inside the epileptic brain. In humans, previous applications of DCM to fMRI data in epilepsy (Hamandi et al., 2008; Klamer et al., 2015, 2018; Murta et al., 2012; Vaudano et al., 2009, 2012, 2013; Warren et al., 2019) adopted the same assumption and in some of them the DCM findings were validated against icEEG with a good agreement between the “driver” defined by the DCM and the EZ recorded by the invasive monitoring (Murta et al., 2012; Klamer et al., 2015). Additionally, there is good evidence of the validity of this approach in relation to intra-cerebral electrophysiology in rats (David et al., 2008).

These data support the feasibility of this technique for the analysis of the temporal dynamics of the spreading of epileptic activity as recorded from the scalp.

Different concerns have been raised about DCM, particularly in relation to the model selection procedure and validation (Lohmann et al., 2012). Herein, for each patient, we built plausible models guided by the main clinical question, that is to reveal the driver of the pathological activity recorded by EEG during fMRI. Model selection was thus based on information derived from other not-invasive investigations and the clinical judgment on the localization of pEZ. In this way, we respect the premise that DCM should be used to test specific hypotheses rather that an exploratory approach (Friston et al., 2003). Accordingly, we excluded a priori any deactivated cluster within the DMN. This choice is motivated by the observation that DMN regions are not usually considered as focus node for the IED generation. Previous EEG-fMRI studies in presurgical epilepsy population aiming to estimate the power of this method to localize the EZ have similarly excluded the DMN regions from the analysis, giving the uncertain meaning of deactivations outside the epileptic focus (An et al., 2013). Furthermore, the observations of a common pattern of IED-related co-deactivation of the DMN in patients with focal epilepsy, especially TLE, may reflect a non-specific and therefore non-localizing phenomenon (An et al., 2013; Laufs et al., 2007), albeit the causal link between IED and DMN involvement has not yet been extensively investigated. It was proposed that IED might spread from the epileptic focus to the one or more functionally interconnected regions of the DMN, perturbing its function. Activity changes in the DMN could thus be a consequence of the IED effect and have a role in decreasing the cognitive performances in TLE (Kobayashi et al., 2006; Kobayashi et al., 2009; Laufs et al., 2007; McCormick et al., 2013; Cataldi et al., 2013; Coan et al., 2014).

Regarding validation of the DCM findings, for each case, we adopted a multi-level approach. Firstly, we based our assessment on the clinical judgment about the pEZ localization derived from the comprehensive presurgical workup. In clinical practice, particularly in patients with not-informative MRI scan, the clinical decision on the EZ localization is fundamental to guide the surgical plan and/or the icEEG implantation. Thus, a comparison between the clinical and the DCM output might be of

519 importance for evaluating the applicability of this approach for clinicians. At this level, we found
520 concordant findings with the DCM results in the majority of our patients (70%). Noteworthy, almost
521 all the patients in our cohort had a structural lesion on the MRI scan which has strongly influenced
522 and maybe simplified the clinical decision about the EZ localization. An interesting future study using
523 DCM on fMRI would focus on a cohort of MRI negative cases in whom the EZ is for definition more
524 complex to be localized (Rossi Sebastiano et al., 2020). Patient #2 of our cohort is a paradigmatic
525 example (**Figure S3**). In this MRI negative epilepsy case, the presurgical investigations end up with
526 discrepant findings: while the scalp EEG and ictal semiology point toward a temporal lateral onset,
527 interictal FDG-PET was more consistent with a temporo-occipital focus. The EEG-fMRI
528 demonstrated multiple areas of BOLD changes covering the temporal, frontal and parietal lobes. In
529 this contest, the DCM approach identified correctly the epileptic nodes as subsequently validated by
530 surgery and confirmed by the post-surgical outcome.
531 As a second step, the DCM findings were independently validated by comparison with the surgical
532 data, particularly clinical outcome. Surgery was performed in 6/10 patients. The remaining 4 cases
533 presented a clear brain lesion (2 FCD, one epidermoid cyst, one DNET) well known to be
534 epileptogenic (Bernasconi et al., 2019; Wang et al., 2020) and in all of them, DCM revealed a driver
535 concordant with the lesion observed in MRI. A previous EEG-fMRI study in focal epilepsy
536 considered a focal lesion on MRI as a criterion for independent validation of fMRI findings (Pittau
537 et al., 2012). Among the patients who underwent SEEG/surgery, a positive independent validation
538 was obtained in the 66% (4/6) of the patients. Interestingly in two out of operated patients (Patients
539 #7,10) with invalid DCM results, the long-term surgery outcome (24 and 36 months respectively)
540 was poor and the DCM findings indicated a driver outside the region of surgical resection. A possible
541 simple explanation for this finding is that the EZ is located outside the area of resection but could
542 correspond to the driver we identified.
543
544

4.3 Methodological Considerations

4.3.1 EEG-fMRI

We have employed a rigid and reliable approach to ensure that regional BOLD changes explained by motion are not considered as effects of interest, by incorporating these features into the GLM model. This methodology replicates previous EEG-fMRI studies from ours (Mirandola et al., 2013; Vaudano et al., 2013; Meletti et al., 2015), and others groups in patients with focal epilepsy (Thornton et al., 2010; Thornton et al., 2010; Thornton et al., 2011; Coan et al., 2016; Markoula et al., 2018). No dataset was discarded because of motion.

The majority of our patients had structural MRI lesions, represented mostly by malformations of cortical development. Several evidences support the feasibility and reliability of the IED-related EEG-fMRI in case of FCD, with a high level of concordance between the BOLD response and the lesion (Archer et al., 2006; Tyvaert et al., 2008; Vaudano et al., 2013; Coan et al., 2016; Pittau et al., 2017) and the SOZ as revealed by icEEG (Thornton et al., 2011; Khoo et al., 2017, 2018). Similar performances were observed for patients with grey matter heterotopia (Kobayashi et al., 2006; Tyvaert et al., 2008; Archer et al., 2010) and polymicrogyria (Kobayashi et al., 2005). As far as DCM on fMRI data, available published data in focal epilepsy have been performed mostly in patients with structural MRI lesion, like FCD (Vaudano et al., 2013), hypothalamic hamartoma (Murta et al., 2012) and hippocampal sclerosis (Hamandi et al., 2008). In all these cases, the DCM applied to fMRI maps demonstrated to be feasible and valid. The co-registration between EPI and anatomical images might be problematic due to the EPI signal dropout at the brain–cerebrospinal fluid–air interfaces; structural lesions could also be of concerns in relation to the co-registration process. In the present work, we addressed this issue by inspecting case by case the good performance of every co-registration step described previously, particularly the overlap between the mean EPI and the pre-operative/post-operative 3D-T1 images. Additionally, in line with previous reports (Coan et al., 2016; Thornton et al., 2011), we allowed a distance up to 2cm to account for displacement between the pEZ/SEEG/resections' margin and the BOLD clusters. This is motivated by the observation that

571 although fMRI is a reliable technique, there can be a spatial difference as high as 10 times its plane
572 resolution, compared to electrophysiologically defined activity (Disbrow et al., 2000).
573
574 4.3.2 DCM model architectures
575 The DCM described findings are limited to the model space specified for each patient. In this regard,
576 we opted for the minimal (from the viewpoint of competing driver hypotheses), set of models, and
577 chose the simplest model architecture including linear and bilinear terms. The decision to include a
578 modulator effect of IED on nodes connections (i.e. bilinear terms) is due to previous studies for our
579 and other groups (Murta et al., 2012; Vaudano et al., 2013) in which different models (with and
580 without modulatory effects) were compared and the bilinear models (i.e. IED act as modulator of the
581 nodes connections) demonstrated an increased likelihood compared with the linear ones. As
582 additional remark, we did not investigate in the models the directionality of connectivity between the
583 nodes and we assumed that the selected ROIs are fully intrinsic connected. Measures of structural
584 connectivity, as obtained by diffusion MRI and probabilistic tractography, have been recently used
585 to inform the DCM structural connectivity parameters at group level with improving inference about
586 the effective connectivity in term of models' evidence (Stephan et al., 2009; Sokolov et al., 2019).
587 Probabilistic approaches have shown indeed that the higher the likelihood that a given connection
588 exists anatomically, the larger the prior variance of the corresponding effective connectivity, making
589 easier for the parameter to deviate from zero and therefore representing a stronger connection
590 (Stephan et al., 2009). Interestingly and in support of this, previous data demonstrated a good
591 correspondence between tractography analysis and the pathway of epileptic activity propagation as
592 revealed by the DCM on IED-related fMRI (Hamandi et al., 2008). Up to know however, tractography
593 information have not been used to inform the connectivity effective parameters in patients with
594 epilepsy. Despite these preliminary evidence and proposed method (Sokolov et al., 2019), further
595 studies are needed to implement the multimodal integration approach in the clinical setting and at
596 individual level.

4.4 Limitations

Firstly, since not all the investigated patients underwent surgery and/or SEEG, the DCM findings lack validation and confirmation for these cases. Noteworthy, in the real-life scenario, when not available surgery or icEEG, the clinical judgment (based on not invasive information) is considered the gold standard for the EZ localization and it is widely used for validation of EEG-fMRI IED mapping results in terms of spatial concordance (Pittau et al., 2012; Yamazoe et al., 2019; Kowalczyk et al., 2020). Secondly, the number of patients investigated with DCM is relatively small and further studies on larger groups of epilepsy patients with confirmed EZ (by SEEG/surgery and/or clinical outcome) are needed to validate our preliminary findings. Thirdly, patients are heterogenous regarding the epilepsy syndrome and related pathology, preventing to model the effective connectivity at group or subgroup level. Of note, the main aim of the present project was to test the usefulness of the DCM approach on fMRI data acquired in consecutive patients, candidate to surgery regardless the epilepsy or seizures type. In this scenario, fMRI and DCM analyses are essentially at single subject's level so the findings can be discussed in relation to the patient only. However, by collecting and analyzed more fMRI datasets using a similar methodological approach would allow to speculate about the validity of the DCM in specific epilepsy clinical and etiological subtypes. Finally, further studies on a larger cohort of patients might address the specificity and sensibility of this approach, thus including also analyses on discordant maps.

4.5 Clinical Significance and Conclusion

The capability of EEG-fMRI to reveal the epileptogenic zone in focal epilepsies has already been documented. However, researchers and clinicians often deal with IED-related fMRI maps that consist of multiple and/or widespread clusters in which the global maxima or primary cluster does not correspond to the epileptogenic zone. This is of concern specially in patients with not-lesional MRI or inconclusive presurgical assessment. In this scenario, we propose that DCM might offer a useful

623 approach helping to interpret these maps by inferring the causal role of its nodes. The present study
624 is the first work that applies this approach to consecutive cases of surgically remediable epilepsies.
625 Overall, our findings support the applicability of DCM on interictal fMRI data, therefore adding
626 evidence on the clinical relevance of the EEG-fMRI as part of the epilepsy presurgical work-up.
627 Additionally, the present work underlines the potential usefulness of effective connectivity analyses
628 to investigate the epileptic networks and to help identifying the EZ in complex cases.

BIBLIOGRAPHY

Archer JS, Abbott DF, Masterton RAJ, Palmer SM, Jackson GD. Functional MRI interactions between dysplastic nodules and overlying cortex in periventricular nodular heterotopia. Epilepsy Behav EB 2010;19(4):631-4.

Aghakhani Y, Beers CA, Pittman DJ, Gaxiola-Valdez I, Goodyear BG, Federico P. Co-localization between the BOLD response and epileptiform discharges recorded by simultaneous intracranial EEG-fMRI at 3 T. NeuroImage Clin 2015;7:755-63.

An D, Fahoum F, Hall J, Olivier A, Gotman J, Dubeau F. Electroencephalography/functional magnetic resonance imaging responses help predict surgical outcome in focal epilepsy. Epilepsia 2013;54(12):2184-94.

Avanzini G, Manganotti P, Meletti S, Moshé SL, Panzica F, Wolf P, et al. The system epilepsies: a pathophysiological hypothesis. Epilepsia 2012;53(5):771-8.

Avanzini P, Vaudano AE, Vignoli A, Ruggieri A, Benuzzi F, Darra F, et al. Low frequency mu-like activity characterizes cortical rhythms in epilepsy due to ring chromosome 20. Clin Neurophysiol Off J Int Fed Clin Neurophysiol 2014;125(2):239-49.

Bartolomei F, Lagarde S, Wendling F, McGonigal A, Jirsa V, Guye M, et al. Defining epileptogenic networks: Contribution of SEEG and signal analysis. Epilepsia 2017;58(7):1131-47

Bénar C-G, Grova C, Kobayashi E, Bagshaw AP, Aghakhani Y, Dubeau F, et al. EEG-fMRI of epileptic spikes: concordance with EEG source localization and intracranial EEG. NeuroImage 2006;30(4):1161-70.

Bernasconi A, Cendes F, Theodore WH, Gill RS, Koepp MJ, Hogan RE, et al. Recommendations for the use of structural magnetic resonance imaging in the care of patients with epilepsy: A consensus report from the International League Against Epilepsy Neuroimaging Task Force. Epilepsia 2019;60(6):1054-1068.

Blumcke I, Spreafico R, Haaker G, Coras R, Kobow K, Bien CG, et al. Histopathological Findings in Brain Tissue Obtained during Epilepsy Surgery. N Engl J Med 2017;377(17):1648-56.

Cardinale F, Rizzi M, Vignati E, Cossu M, Castana L, d'Orio P, et al. Stereoelectroencephalography: retrospective analysis of 742 procedures in a single centre. Brain J Neurol. 2019;142(9):2688-704.

Cataldi M, Avoli M, de Villers-Sidani E. Resting state networks in temporal lobe epilepsy. Epilepsia 2013;54(12):2048-59.

Chaudhary UJ, Carmichael DW, Rodionov R, Thornton RC, Bartlett P, Vulliemoz S, et al. Mapping preictal and ictal haemodynamic networks using video-electroencephalography and functional imaging. Brain J Neurol 2012;135(Pt 12):3645-63.

Coan AC, Campos BM, Beltramini GC, Yasuda CL, Covolan RJM, Cendes F. Distinct functional and structural MRI abnormalities in mesial temporal lobe epilepsy with and without hippocampal sclerosis. Epilepsia 2014;55(8):1187-96.

679 Coan AC, Chaudhary UJ, Frédéric Grouiller, Campos BM, Perani S, De Ciantis A, et al. EEG-fMRI in
680 the presurgical evaluation of temporal lobe epilepsy. J Neurol Neurosurg Psychiatry. 2016;87(6):642-
681 9.
682
683 David O, Guillemain I, Saillet S, Reyt S, Deransart C, Segebarth C, et al. Identifying neural drivers
684 with functional MRI: an electrophysiological validation. PLoS Biol 2008;6(12):2683-97.
685
686 Disbrow EA, Slutsky DA, Roberts TP, Krubitzer LA. Functional MRI at 1.5 tesla: a comparison of the
687 blood oxygenation level-dependent signal and electrophysiology. Proc Natl Acad Sci U S A
688 2000;97(17):9718-23.
689
690 Duez L, Tankisi H, Hansen PO, Sidenius P, Sabers A, Pinborg LH, et al. Electromagnetic source
691 imaging in presurgical workup of patients with epilepsy: A prospective study. Neurology
692 2019;92(6):e576-86.
693
694 Duncan JS, Winston GP, Koepp MJ, Ourselin S. Brain imaging in the assessment for epilepsy surgery.
695 Lancet Neurol. 2016;15(4):420-33.
696
697 Engel J, editor. Surgical treatment of the epilepsies. 2nd ed. New York: Raven Press; 1993. 786 p.
698
699 Fedorov A, Beichel R, Kalpathy-Cramer J, Finet J, Fillion-Robin J-C, Pujol S, et al. 3D Slicer as an
700 image computing platform for the Quantitative Imaging Network. Magn Reson Imaging
701 2012;30(9):1323-41.
702
703 Friston KJ, Williams S, Howard R, Frackowiak RS, Turner R. Movement-related effects in fMRI time-
704 series. Magn Reson Med. 1996;35(3):346-55.

Friston KJ, Harrison L, Penny W. Dynamic causal modelling. NeuroImage 2003 Aug;19(4):1273-302.

González Otárula KA, Khoo HM, von Ellenrieder N, Hall JA, Dubeau F, Gotman J. Spike-related haemodynamic responses overlap with high frequency oscillations in patients with focal epilepsy. Brain J Neurol 2018;141(3):731-43.

Gotman J, Pittau F. Combining EEG and fMRI in the study of epileptic discharges. Epilepsia 2011;52 Suppl 4(Suppl 4):38-42.

Hamandi K, Salek-Haddadi A, Laufs H, Liston A, Friston K, Duncan JS, Fish DR, Lemieux L. EEG-fMRI of idiopathic and secondarily generalized epilepsies. NeuroImage, 31(4): 1700-10, 2006.

Hamandi K, Powell HWR, Laufs H, Symms MR, Barker GJ, Parker GJM, et al. Combined EEG-fMRI and tractography to visualise propagation of epileptic activity. J Neurol Neurosurg Psychiatry. 2008;79(5):594-7.

Jehi L. The Epileptogenic Zone: Concept and Definition. Epilepsy Curr 2018;18(1):12-6.

Kahan J, Foltynie T. Understanding DCM: Ten simple rules for the clinician. NeuroImage 2013;83:542-9.

Kalilani L, Sun X, Pelgrims B, Noack-Rink M, Villanueva V. The epidemiology of drug-resistant epilepsy: A systematic review and meta-analysis. Epilepsia 2018;59(12):2179-93.

730 Kane N, Acharya J, Beniczky S, Caboclo L, Finnigan S, Kaplan PW, et al. A revised glossary of terms
731 most commonly used by clinical electroencephalographers and updated proposal for the report format
732 of the EEG findings. Revision 2017. Clin Neurophysiol Pract 2017;2:170-85.
733
734 Khoo HM, Hao Y, von Ellenrieder N, Zazubovits N, Hall J, Olivier A, et al. The hemodynamic response
735 to interictal epileptic discharges localizes the seizure-onset zone. Epilepsia 2017;58(5):811-23.
736 Khoo HM, von Ellenrieder N, Zazubovits N, He D, Dubeau F, Gotman J. The spike onset zone: The
737 region where epileptic spikes start and from where they propagate. Neurology 2018;91(7):e666-74.
738
739 Klamer S, Rona S, Elshahabi A, Lerche H, Braun C, Honegger J, et al. Multimodal effective
740 connectivity analysis reveals seizure focus and propagation in musicogenic epilepsy. NeuroImage
741 2015;113:70-7.
742
743 Klamer S, Ethofer T, Torner F, Sahib AK, Elshahabi A, Marquetand J, et al. Unravelling the brain
744 networks driving spike-wave discharges in genetic generalized epilepsy-common patterns and
745 individual differences. Epilepsia Open 2018;3(4):485-94.
746
747 Kobayashi E, Bagshaw AP, Jansen A, Andermann F, Andermann E, Gotman J, et al. Intrinsic
748 epileptogenicity in polymicrogyric cortex suggested by EEG-fMRI BOLD responses. Neurology
749 2005;64(7):1263-6.
750
751 Kobayashi E, Bagshaw AP, Grova C, Gotman J, Dubeau F. Grey matter heterotopia: what EEG-fMRI
752 can tell us about epileptogenicity of neuronal migration disorders. Brain 2006;129(2):366-74.
753

754 Kobayashi E, Grova C, Tyvaert L, Dubeau F, Gotman J. Structures involved at the time of temporal
755 lobe spikes revealed by interindividual group analysis of EEG/fMRI data. Epilepsia 2009;50(12):2549-
756 56.
757
758 Kobayashi E, Bagshaw AP, Grova C, Dubeau F, Gotman J. Negative BOLD responses to epileptic
759 spikes. Hum Brain Mapp 2006;27(6):488–97.
760
761 Kowalczyk MA, Omidvarnia A, Abbott DF, Tailby C, Vaughan DN, Jackson GD. Clinical benefit of
762 presurgical EEG-fMRI in difficult-to-localize focal epilepsy: A single-institution retrospective review.
763 Epilepsia 2020;61(1):49-60.
764
765 Kowalczyk MA, Omidvarnia A, Dhollander T, Jackson GD. Dynamic analysis of fMRI activation
766 during epileptic spikes can help identify the seizure origin. Epilepsia 2020;61(11):2558-71.
767
768 Kozák LR, van Graan LA, Chaudhary UJ, Szabó ÁG, Lemieux L. ICN_Atlas: Automated description
769 and quantification of functional MRI activation patterns in the framework of intrinsic connectivity
770 networks. NeuroImage 2017;163:319-41.
771
772 Kural MA, Tankisi H, Duez L, Sejer Hansen V, Udupi A, Wennberg R, et al. Optimized set of criteria
773 for defining interictal epileptiform EEG discharges. Clin Neurophysiol 2020;131(9):2250-4.
774
775 Laufs H, Hamandi K, Salek-Haddadi A, Kleinschmidt AK, Duncan JS, Lemieux L. Temporal lobe
776 interictal epileptic discharges affect cerebral activity in “default mode” brain regions. Hum Brain Mapp
777 2007;28(10):1023-32.
778

779 Lemieux L, Laufs H, Carmichael D, Paul JS, Walker MC, Duncan JS. Noncanonical spike-related
780 BOLD responses in focal epilepsy. Hum Brain Mapp 2008;29(3):329-45.
781
782 Liu J, Liu B, Zhang H. Surgical versus medical treatment of drug-resistant epilepsy: A systematic
783 review and meta-analysis. Epilepsy Behav 2018;82:179-88.
784
785 Lohmann G, Erfurth K, Müller K, Turner R. Critical comments on dynamic causal modelling.
786 NeuroImage. 2012;59(3):2322-9
787
788 Markoula S, Chaudhary UJ, Perani S, Ciantis AD, Yadee T, Duncan JS, et al. The impact of mapping
789 interictal discharges using EEG-fMRI on the epilepsy presurgical clinical decision making process: A
790 prospective study. Seizure - Eur J Epilepsy 2018;61:30-7.
791
792 Meletti S, Vaudano AE, Tassi L, Caruana F, Avanzini P. Intracranial time–frequency correlates of
793 seizure-related negative BOLD response in the sensory-motor network. Clin Neurophysiol.
794 2015;126(4):847-9.
795
796 Mirandola L, Cantalupo G, Vaudano AE, Avanzini P, Ruggieri A, Pisani F, et al. Centrotemporal spikes
797 during NREM sleep: The promoting action of thalamus revealed by simultaneous EEG and fMRI
798 coregistration. Epilepsy Behav Case Rep 2013;1:106-9.
799
800 Moran RJ, Stephan KE, Kiebel SJ, Rombach N, O'Connor WT, Murphy KJ, et al. Bayesian estimation
801 of synaptic physiology from the spectral responses of neural masses. NeuroImage 2008;42(1):272-84.
802
803 Murta T, Leal A, Garrido MI, Figueiredo P. Dynamic Causal Modelling of epileptic seizure propagation
804 pathways: A combined EEG-fMRI study. NeuroImage 2012;62(3):1634-42.

Narizzano M, Arnulfo G, Ricci S, Toselli B, Tisdall M, Canessa A, et al. SEEG assistant: a 3DSlicer extension to support epilepsy surgery. BMC Bioinformatics 2017 Dec 18(1):124.

Penny WD, Stephan KE, Mechelli A, Friston KJ. Comparing dynamic causal models. NeuroImage 2004;22(3):1157-72.

Pittau F, Dubeau F, Gotman J. Contribution of EEG/fMRI to the definition of the epileptic focus. Neurology. 2012;78(19):1479-87.

Pittau F, Ferri L, Fahoum F, Dubeau F, Gotman J. Contributions of EEG-fMRI to Assessing the Epileptogenicity of Focal Cortical Dysplasia. Front Comput Neurosci 2017;11.

Rampp S, Stefan H, Wu X, Kaltenhäuser M, Maess B, Schmitt FC, et al. Magnetoencephalography for epileptic focus localization in a series of 1000 cases. Brain J Neurol 2019;142(10):3059-71.

Ray KL, McKay DR, Fox PM, Riedel MC, Uecker AM, Beckmann CF, et al. ICA model order selection of task co-activation networks. Front Neurosci 2013;7.

Rossi Sebastiano D, Tassi L, Duran D, Visani E, Gozzo F, Cardinale F et al. Identifying the epileptogenic zone by four non-invasive imaging techniques versus stereo-EEG in MRI-negative pre-surgery epilepsy patients. Clinical Neurophysiology 2020;131(8):1815-1823.

Salek-Haddadi A, Diehl B, Hamandi K, Merschhemke M, Liston A, Friston K, et al. Hemodynamic correlates of epileptiform discharges: An EEG-fMRI study of 63 patients with focal epilepsy. Brain Res 2006;1088(1):148-66.

831

832 Sokolov AA, Zeidman P, Erb M, Ryvlin P, Pavlova MA, Friston KJ. Linking structural and effective
833 brain connectivity: structurally informed Parametric Empirical Bayes (si-PEB). Brain Struct Funct
834 2019;224(1):205-17.
835 Stephan KE, Friston KJ. Analyzing effective connectivity with functional magnetic resonance imaging.
836 Wiley Interdisciplinary Reviews: Cognitive Science 2010;1(3):446-459.
837
838 Stephan KE, Tittgemeyer M, Knösche TR, Moran RJ, Friston KJ. Tractography-based priors for
839 dynamic causal models. NeuroImage. 2009;47(4):1628-38.
840
841 Thornton R, Laufs H, Rodionov R, Cannadathu S, Carmichael DW, Vulliemoz S, et al. EEG correlated
842 functional MRI and postoperative outcome in focal epilepsy. J Neurol Neurosurg Psychiatry
843 2010(a);81(8):922-7.
844
845 Thornton RC, Rodionov R, Laufs H, Vulliemoz S, Vaudano A, Carmichael D, et al. Imaging
846 haemodynamic changes related to seizures: Comparison of EEG-based general linear model,
847 independent component analysis of fMRI and intracranial EEG. NeuroImage 2010(b);53(1):196-205.
848
849 Thornton R, Vulliemoz S, Rodionov R, Carmichael DW, Chaudhary UJ, Diehl B, et al. Epileptic
850 networks in focal cortical dysplasia revealed using electroencephalography-functional magnetic
851 resonance imaging. Ann Neurol 2011;70(5):822-37.
852
853 Tyvaert L, Hawco C, Kobayashi E, LeVan P, Dubeau F, Gotman J. Different structures involved during
854 ictal and interictal epileptic activity in malformations of cortical development: an EEG-fMRI study.
855 Brain J Neurol 2008;131(Pt 8):2042-60.
856

857 Vakharia VN, Duncan JS, Witt J-A, Elger CE, Staba R, Engel J. Getting the best outcomes from
858 epilepsy surgery: Epilepsy Surgery Outcomes. Ann Neurol 2018;83(4):676-90.
859
860 Varotto G, Tassi L, Franceschetti S, Spreafico R, Panzica F. Epileptogenic networks of type II focal
861 cortical dysplasia: A stereo-EEG study. NeuroImage 2012;61(3):591-8.
862
863 Vaudano AE, Laufs H, Kiebel SJ, Carmichael DW, Hamandi K, Guye M, et al. Causal hierarchy within
864 the thalamo-cortical network in spike and wave discharges. PloS One 2009;4(8):e6475.
865
866 Vaudano AE, Carmichael DW, Salek-Haddadi A, Rampp S, Stefan H, Lemieux L, et al. Networks
867 involved in seizure initiation. A reading epilepsy case studied with. Neurology 2012;79(3):249-53.
868
869 Vaudano AE, Avanzini P, Tassi L, Ruggieri A, Cantalupo G, Benuzzi F, et al. Causality within the
870 Epileptic Network: An EEG-fMRI Study Validated by Intracranial EEG. Front Neurol 2013;4.
871
872 Wang I, Bernasconi A, Bernhardt B, Blumenfeld H, Cendes F, Chinvarun Y et al. MRI essentials in
873 epileptology: A review from the ILAE Imaging Taskforce. Epileptic Disorders 2020;22(4): 421-437.
874
875 Warren AEL, Harvey AS, Vogrin SJ, Bailey C, Davidson A, Jackson GD, et al. The epileptic network
876 of Lennox-Gastaut syndrome: Cortically driven and reproducible across age. Neurology
877 2019;93(3):e215-26.
878
879 Watanabe S, Dubeau F, Zazubovits N, Gotman J. Temporal lobe spikes: EEG-fMRI contributions to
880 the “mesial vs. lateral” debate. Clin Neurophysiol 2017 128(6):986-91.
881

882 Whelan CD, Altmann A, Botía JA, Jahanshad N, Hibar DP, Absil J, et al. Structural brain abnormalities
883 in the common epilepsies assessed in a worldwide ENIGMA study. Brain 2018;141(2):391-408.
884
885 Yamazoe T, von Ellenrieder N, Khoo HM, Huang Y-H, Zazubovits N, Dubeau F, et al. Widespread
886 interictal epileptic discharge more likely than focal discharges to unveil the seizure onset zone in
887 EEG-fMRI. Clin Neurophysiol 2019;130(4):429-38.
888
889 Zijlmans M, Zweiphenning W, van Klink N. Changing concepts in presurgical assessment for
890 epilepsy surgery. Nat Rev Neurol 2019;15(10):594–606.
891

Figures Legend

Figure 1. DCM findings. **A**: DCM findings in relation to the pEZ; **B**: DCM findings in relation to pEZ across the different epileptic syndromes. FLE: Frontal Lobe Epilepsy; TLE: Temporal Lobe Epilepsy; PLE: Parietal Lobe Epilepsy. See text for details.

Figure 2. Example of "*concordant, SEEG/surgery-validated and confirmed*" DCM result. Patient #3. **A**: Left: Representative segment of scalp EEG showing IED over the right frontal and frontal-temporal leads. EEG is displayed in bipolar montage. Right: IED-related fMRI results overlaid onto high-resolution 3D-T1 image (axial, coronal, sagittal slices). Three clusters of IED-related BOLD signal increase ($p < 0.05$, FWE) in the left postcentral (global maxima), right postcentral and right entorhinal cortices. **B**: Left: DCM model architecture: three ROIs are forward and backward connected (intrinsic connections are not shown for illustrative purposes). IED were considered as autonomous input to each of the three regions, one at a time (*grey arrow*). The bilinear terms are represented as solid *green arrows*. Right: DCM Bayesian model selection results: relative Log-evidence and Posterior Probability for the three models compared using FFX BMS show the winning model as Model 1 [p(m|Y)=0,99]. The log-evidence difference between the three models was significant, showing a driver in the right postcentral cortex. **C:** SEEG electrode positions and EEG-fMRI findings overlaid onto the presurgical reconstructed right hemisphere pial surface. The most active electrodes were located in the centro-parietal operculum (electrode S), supramarginal gyrus and inferior parietal lobuli (electrodes X, W, F) and anterior part of the inferior parietal lobuli (electrode P). **D:** Post-surgical 3D-T1 MRI coronal and sagittal slices with EEG-fMRI findings and intracranial electrodes overlaid. Note that the fMRI cluster is included in the resection area. R: right; L: left. Rh: Right Hemisphere; sMRI: Structural MRI.

Figure 3. Example of "*discordant, surgery-invalidated but unconfirmed*" DCM result. Patient #7. **A**: Representative segment of scalp EEG showing IED over the left frontal-central and central-parietal

regions. EEG is displayed in bipolar montage. **B**: Top: structural MRI scan (3D-T1) shows thickening and blurring of the grey-white matter junction over the left superior parietal gyrus (red circles) suggestive of FCD. Bottom: IED-related fMRI results overlaid onto the high-resolution pre-surgical 3D-T1 image (axial and coronal slices) revealed ($p < 0.05$, small volume correction and family-wise error corrected) three main clusters of BOLD signal increase: the left post-central gyrus (global maxima), the left paracentral gyrus and the right post-central gyrus. **C**: Left: DCM model architecture. Three ROIs are forward and backward connected (intrinsic connections are not shown for illustrative purposes). IED were considered as autonomous input to each of the three regions, one at a time (*grey arrow*). The bilinear terms are represented as solid *green arrows.* Right: DCM Bayesian model selection results: relative log-evidence and posterior probability for the three models compared using FFX BMS show the winning model as Model 3 [$p(m|Y)=0,99$]. The log-evidence difference between these three models was significant. **D**: Presurgical IED-related fMRI findings overlaid onto post-surgical high-resolution 3D T1scan. R: right; L: left. FCD: Focal Cortical Dysplasia; sMRI: Structural MRI.

Figure 4. Example of "*inconclusive*" DCM result. Patient #9. **Panel A**. Representative segment of EEG showing IED over the left frontal-temporal regions. EEG is displayed in bipolar montage. **B**: Top: structural MRI scan (3D-T1) shows a localized left amygdala-hippocampal lesion suggestive of DNET (red circles). Bottom: IED-related fMRI results overlaid onto high-resolution presurgical 3D-T1 image (axial and coronal slices) revealed two clusters of signal increases ($p < 0.05$, small volume correction and family-wise error corrected) in the left hippocampus extending to the amygdala (global maxima) and the homolateral middle temporal gyrus. **C:** Left: DCM models' architecture: two ROIs are structurally (forward and backward) connected (intrinsic connections are not shown in the models for illustrative purposes). IED were considered as autonomous input to each of the two regions, one at a time (*grey arrow*). The bilinear terms are represented as solid *green arrows*. Right: DCM Bayesian model selection results: relative log-evidence and posterior probability for the two models

compared using FFX BMS found Model 1 to be more likely [*p*(m|Y)=0,70] but below the significance threshold. R: right; L: left; sMRI: Structural MRI.

Figure S1. Overview of the EEG-fMRI results. IED: Interictal Epileptiform Discharges; *N*: Null; *C*: Concordant; *C*+: Concordant Plus; *D*+: Discordant Plus; *D*: Discordant.

Figure S2. Patient with "*concordant*" DCM result. Patient #1. **A**: Representative segment of scalp EEG showing IED over the left frontal-central regions. EEG is displayed in bipolar montage. **B**: Structural MRI (top: high-resolution 3D FLAIR; bottom: high-resolution 3D-T1 MRI showing a deep left caudal middle frontal gyrus with blurring of the surrounding grey-white matter junction, suggestive for FCD (red circles). **C:** IED-related fMRI results overlaid onto the high-resolution presurgical FLAIR image (axial and coronal slices) demonstrated two significant (p<0,05 FWE) clusters of signal increase: the left superior frontal gyrus (global maxima) and the homolateral middle frontal gyrus. **D:** Left Image: DCM models' architecture: two ROIs are structurally (forward and backward) connected (intrinsic connections are not shown in the models for illustrative purposes). IED were considered as autonomous input to each of the two regions, one at a time (*grey arrow*). The bilinear terms are represented as solid *green arrows*. Right image: DCM Bayesian model selection results: relative log-evidence and posterior probability for the two models compared using FFX BMS show the winning model as Model 2 [p(m|Y)=0,98]. The log-evidence difference between these two models was >3 (hence significant). R: right; L: left; FCD: Focal Cortical Dysplasia; sMRI: Structural MRI.

Figure S3. Patient with "*concordant, SEEG/surgery-validated and confirmed"* DCM result. Patient #2. **A:** Representative segment of scalp EEG showing the marked IED over the right middle temporal regions ("s" refers to the marker of identify spikes after EEG preprocessing). EEG is displayed in bipolar montage. **B:** IED-related fMRI results overlaid onto the high-resolution 3D-T1 (axial,

coronal, sagittal slices) demonstrated a single large cluster of BOLD signal increases (p<0.05, corrected for FWE) over the right middle temporal gyrus extending toward the homolateral supramarginal gyrus and inferior parietal lobule plus smaller blobs over the right posterior cingulate cortex, right superior temporal sulcus and right rostral middle frontal gyrus. Decreases in BOLD signal changes were observed in the DMN lateralized on the right side. The cold blue color identifies BOLD signal decreases while the hot red-yellow color, BOLD signal increases. **C**: Left: DCM models' architecture: four ROIs (derived from the activated BOLD clusters) are structurally (forward and backward) connected (intrinsic connections are not shown in the models for illustrative purposes). IED were considered as autonomous input to each of the four regions, one at a time (*grey arrow*). The bilinear terms are represented as solid *green arrows*. Right: DCM Bayesian model selection results: relative Log-evidence and Posterior Probability for the four models compared using FFX BMS show two winning models: Model 1 [p(m|Y)=0,78] and Model 4 [p(m|Y)=0,17]. The log-evidence difference between Models 1 and 4 was less than 3 (hence not significant), while the difference between Model1&4 and the Model 2&3 was >3, hence significant. **D**: SEEG electrodes position and EEG-fMRI findings overlaid onto the presurgical reconstructed right hemisphere pial surface. Most active electrodes explored the temporo-basal and temporo-occipital regions (D and X), superior and middle temporal cortex (W, U which corresponds to Wernicke area), and the more superficial part of the inferior parietal lobuli (Y). **E**: Post-surgical MRI scan displayed onto 3D T1 coronal and sagittal and axial slices with overlaid the EEG-fMRI findings and intracranial electrodes. Note that the middle temporal fMRI cluster is included in the resection area. **F**: Interictal FDG-PET overlaid onto right hemisphere pial surface together with SEEG electrodes position. The green color identifies hypometabolism. R: right; L: left; Rh: right hemisphere; sMRI: Structural MRI.

Figure S4. Patient with "*concordant, surgery-validated and confirmed"* DCM result. Patient #4. **A:** Top: presurgical 3D-T1 shows a temporal polar and hippocampus FCD (red circles). Bottom: IED-related fMRI results overlaid onto the high-resolution presurgical 3D-T1, axial and coronal slices

997 shown two main clusters of signal increase ($p < 0.05$, small volume correction and family-wise error
998 corrected) in the left insular cortex (global maxima) and in the left temporal pole. **B:** Left: DCM
999 models' architecture: two ROIs are structurally (forward and backward) connected (intrinsic
1000 connections are not shown in the models for illustrative purposes). IED were considered as
1001 autonomous input to each of the two regions, one at a time (*grey arrow*). The bilinear terms are
1002 represented as solid *green arrows*. Right: DCM Bayesian model selection results: relative log-
1003 evidence and posterior probability for the two models compared using FFX BMS show the winning
1004 model as Model 2 [p(m|Y)=0,80]. The log-evidence difference between these two models was >3
1005 (hence significant). **C:** Post-operative FLAIR axial image showing the resection area. R: right; L:
1006 left; sMRI: Structural MRI.
1007
1008 **Figure S5** Patient with "*concordant*" DCM result. Patient #5. **A:** Representative segment of scalp
1009 EEG showing the IED over the right fronto-temporal and middle regions. **B:** ictal EEG shows low-
1010 voltage fast activity over the right middle and posterior temporal leads with diffusion to the
1011 homolateral parieto-occipital regions. The black arrow indicates the timing of ictal clinical semiology
1012 onset. EEGs are displayed in bipolar montage. **C:** Left: structural MRI (high-resolution FLAIR scan,
1013 coronal and sagittal slices) shows a right basal temporal cortex (fusiform gyrus) FCD (red circles).
1014 Right Images: IED-related fMRI results overlaid onto the high-resolution presurgical FLAIR, coronal
1015 and sagittal slices demonstrated two significant ($p<0,05$ FWE) clusters of signal increase: the global
1016 maxima located in the right parietal cortex (inferior parietal gyrus) and a smaller blob in the
1017 homolateral fusiform gyrus. **D:** Left: DCM models' architecture: two ROIs are structurally (forward
1018 and backward) connected (intrinsic connections are not shown in the models for illustrative purposes).
1019 IED were considered as autonomous input to each of the two regions, one at a time (*grey arrow*). The
1020 bilinear terms are represented as solid *green arrows*. Right: DCM Bayesian model selection results:
1021 relative log-evidence and posterior probability for the two models compared using FFX BMS show

1022 the winning model as Model 1 [p(m|Y)=1.00]. The log-evidence difference between these two models
1023 was >3 (hence significant). R: right; L: left; FCD: Focal Cortical Dysplasia; sMRI: Structural MRI.
1024
1025 **Figure S6** Patient with "*concordant*" DCM result. Patient #6. **A:** Structural MRI (top image: high-
1026 resolution 3D-T1; bottom image: high-resolution FLAIR, axial and coronal slices) shows the left
1027 anterior insular epidermoid cyst (red circles). **B:** Representative segment of scalp EEG showing the
1028 marked IED over the left fronto-temporal regions. EEG is displayed in bipolar montage. **C:** IED-
1029 related fMRI results overlaid onto the high-resolution presurgical 3D-T1, axial and coronal slices;
1030 demonstrated two significant (p<0,05 FWE) clusters of signal increase: the global maxima located in
1031 the left inferior frontal gyrus (pars triangularis) and a second blob in the homolateral superior frontal
1032 gyrus. **D:** Left: DCM models' architecture: two ROIs are structurally (forward and backward)
1033 connected (intrinsic connections are not shown in the models for illustrative purposes). IED were
1034 considered as autonomous input to each of the two regions, one at a time (*grey arrow*). The bilinear
1035 terms are represented as solid *green arrows*. Right: DCM Bayesian model selection results: relative
1036 log-evidence and posterior probability for the two models compared using FFX BMS show the
1037 winning model as Model 1 [p(m|Y)=0,99]. The log-evidence difference between these two models
1038 was >3, see text for details. R: right; L: left. sMRI: Structural MRI.
1039
1040
1041 **Figure S7**. Patient with "*concordant, surgery-validated and confirmed"* DCM result. Patient #8. **A:**
1042 Representative segment of scalp EEG showing diffuse IED with a clear prevalence over the left
1043 parieto-temporal leads. EEG is displayed in bipolar montage. **B:** Top: high-resolution FLAIR coronal
1044 and axial slices showing a residual FCD around the surgical cavity involving the left precuneus
1045 concordant with interictal FDG-interictal PET findings (red circles). Bottom: IED-related fMRI
1046 results overlaid onto the high-resolution presurgical FLAIR, axial, coronal and sagittal slices revealed
1047 ($p < 0.05$, small volume correction and family-wise error corrected) two clusters of signal increases

1048 located at the right superior parietal cortex (Global Maxima) and a smaller blob at the left precuneus.
1049 **C:** Left: DCM models' architecture: two ROIs are structurally (forward and backward) connected
1050 (intrinsic connections are not shown in the models for illustrative purposes). IED were considered as
1051 autonomous input to each of the two regions, one at a time (*grey arrow*). The bilinear terms are
1052 represented as solid *green arrows*. Right: DCM Bayesian model selection results: relative log-
1053 evidence and posterior probability for the two models compared using FFX BMS show the winning
1054 model as Model 2 [p(m|Y)=1]. The log-evidence difference between these two models was >3 (hence
1055 significant). **D:** presurgical IED-related fMRI findings overlaid onto post-surgical high-resolution
1056 FLAIR scan. R: right; L: left; FCD: Focal Cortical Dysplasia; sMRI: Structural MRI.
1057
1058 **Figure S8**. Patient with "*discordant, surgery-invalidate but unconfirmed"* DCM result. Patient #10.
1059 **A:** Representative segment of scalp EEG showing focal IED located over the right fronto-central and
1060 centro-parietal leads. EEG is displayed in bipolar montage. **B:** Top: high-resolution presurgical
1061 FLAIR coronal and axial slices show the right temporo-occipital AVM (red circles). Bottom: IED-
1062 related fMRI results overlaid onto high-resolution presurgical FLAIR coronal and axial slices
1063 demonstrated ($p < 0.05$, FWE corrected) four principal cluster of signal increases at the right superior
1064 temporal gyrus (global maxima), right middle temporal gyrus (corresponding to the anterior border
1065 of the MAV lesion), right cuneus and right frontal operculum. **C:** Left: DCM models' architecture:
1066 four ROIs are structurally (forward and backward) connected (intrinsic connections are not shown in
1067 the models for illustrative purposes). IED were considered as autonomous input to each of the four
1068 regions, one at a time (*grey arrow*). The bilinear terms are represented as solid *green arrows*. Right:
1069 DCM Bayesian model selection results: relative log-evidence and posterior probability for the four
1070 models compared using FFX BMS show two winning models, Model 1 [p(m|Y)=0,68] and Model 3
1071 [p(m|Y)=0,31]. The log-evidence difference between these two models was <3 (hence not
1072 significant), while the log-evidence difference between Models 1 and 3 and the others were >3, hence

significant, see text for details. **D:** post-surgical high-resolution FLAIR scan. R: right; L: left. AVM: Arteriovenous Malformation; sMRI: Structural MRI.

Figure 1

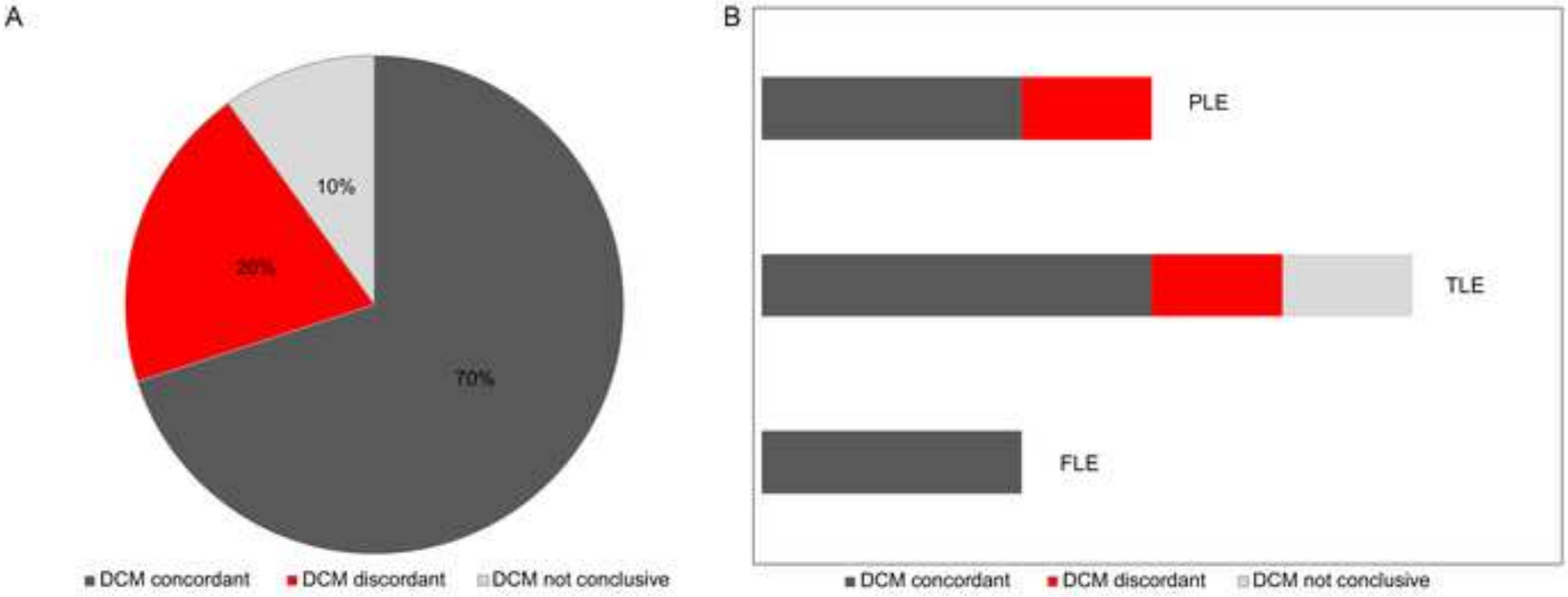

Figure 2

Click here to access/download;Figure;Figure2_R1.tif

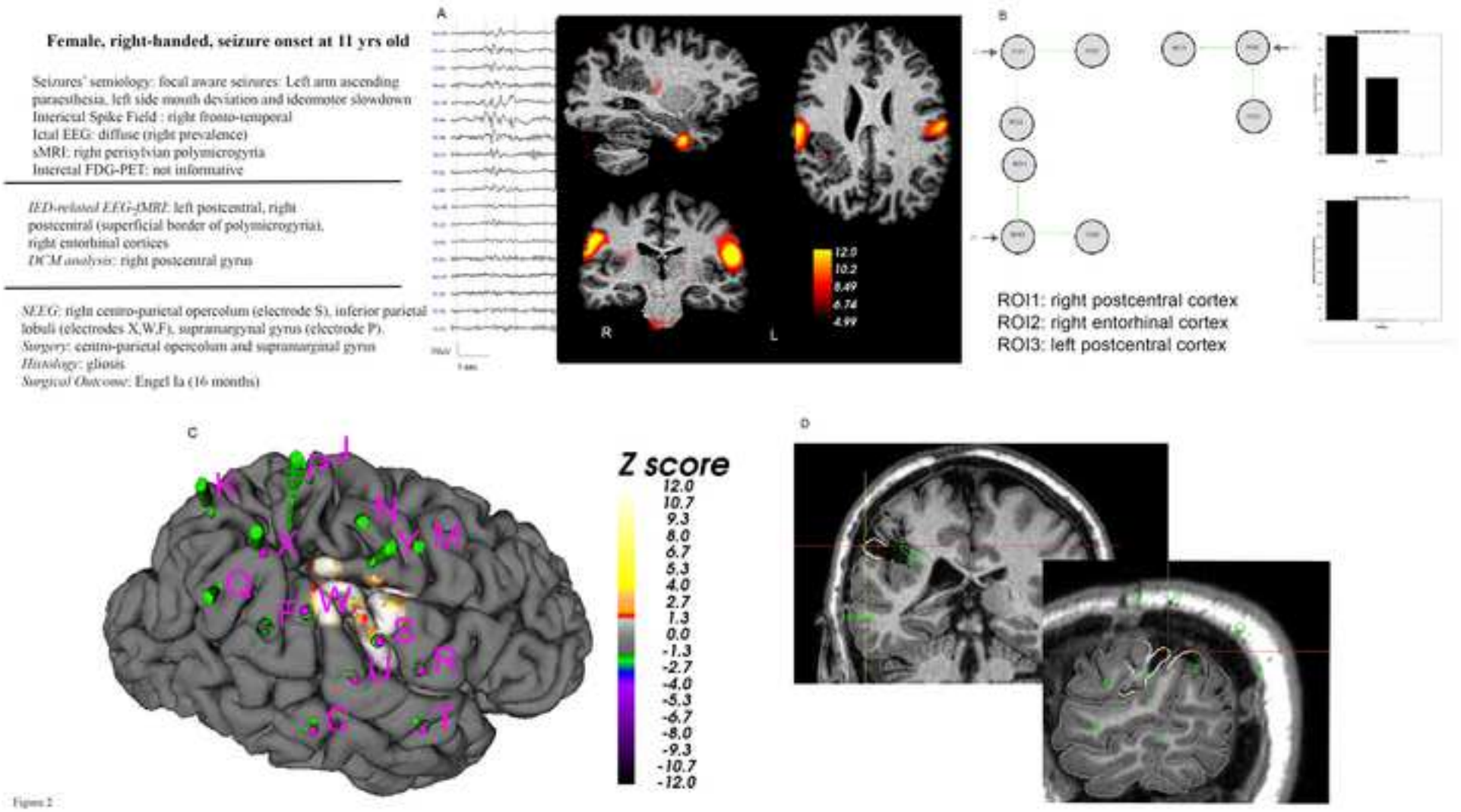

Female, right-handed, seizure onset at 5 yrs old

Seizures' semiology: focal aware seizures: paresthesia involving the right foot and homolateral shoulder, stiffening of the right leg and fall to the floor
Interictal Spike Field : left fronto-central-parietal
Ictal EEG: left fronto-central-parietal
sMRI: left superior-parietal FCD
Interctal FDG-PET: not available

IED-related EEG-fMRI: left postcentral, left paracentral gyrus, right postcentral gyrus
DCM analysis: left paracentral gyrus

Surgery: lesionectomy (left postcentral gyrus)
Histology: FCD IIb.
Surgical Outcome: Engel III (24 months)

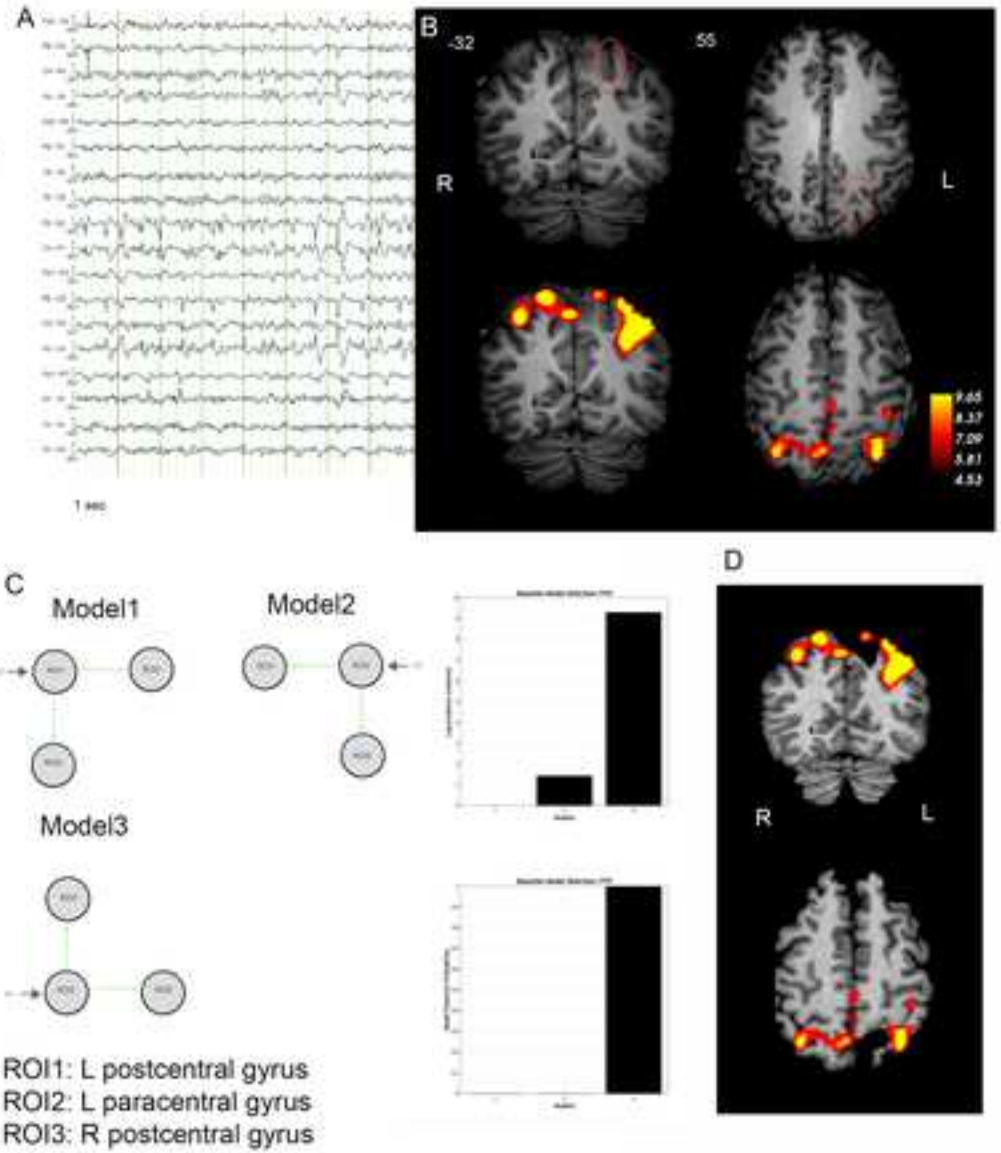

Figure 3

Female, right-handed, seizure onset at 22 yrs old

Seizures' semiology: focal aware seizures: subjective muffled sound sensation, staring and oral automatisms
Interictal Spike Field : left fronto-temporal
Ictal EEG: left fronto-temporal
sMRI: left amygdala-hippocampal DNET
Interctal FDG-PET: not available

IED-related EEG-fMRI: left hippocampus, left middle temporal gyrus
DCM analysis: left hippocampus and left middle temporal gyrus

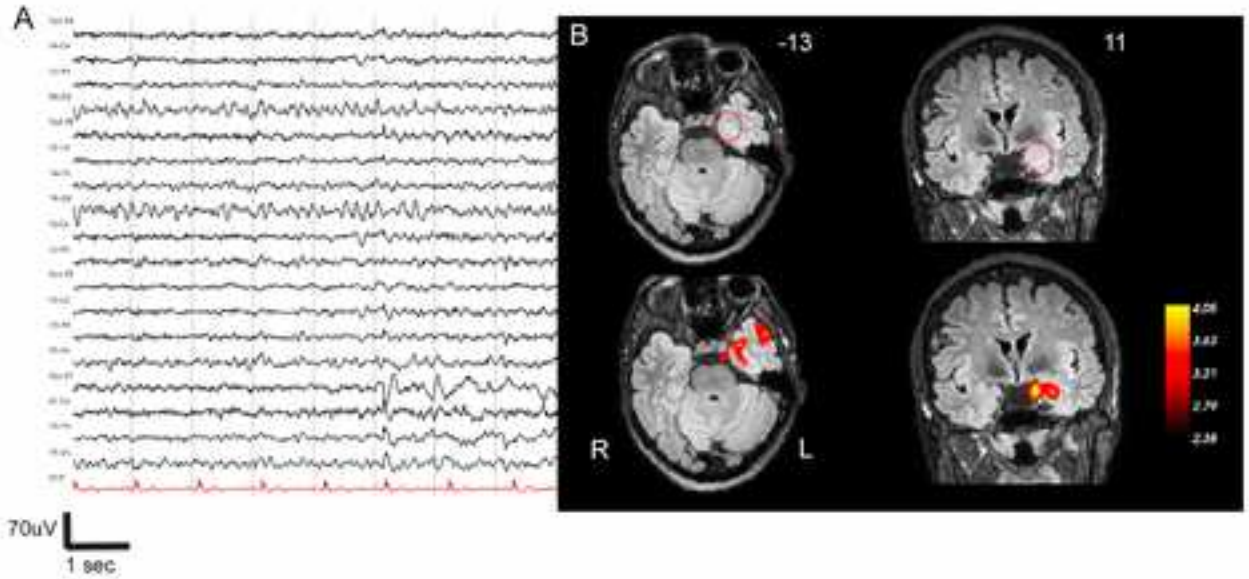

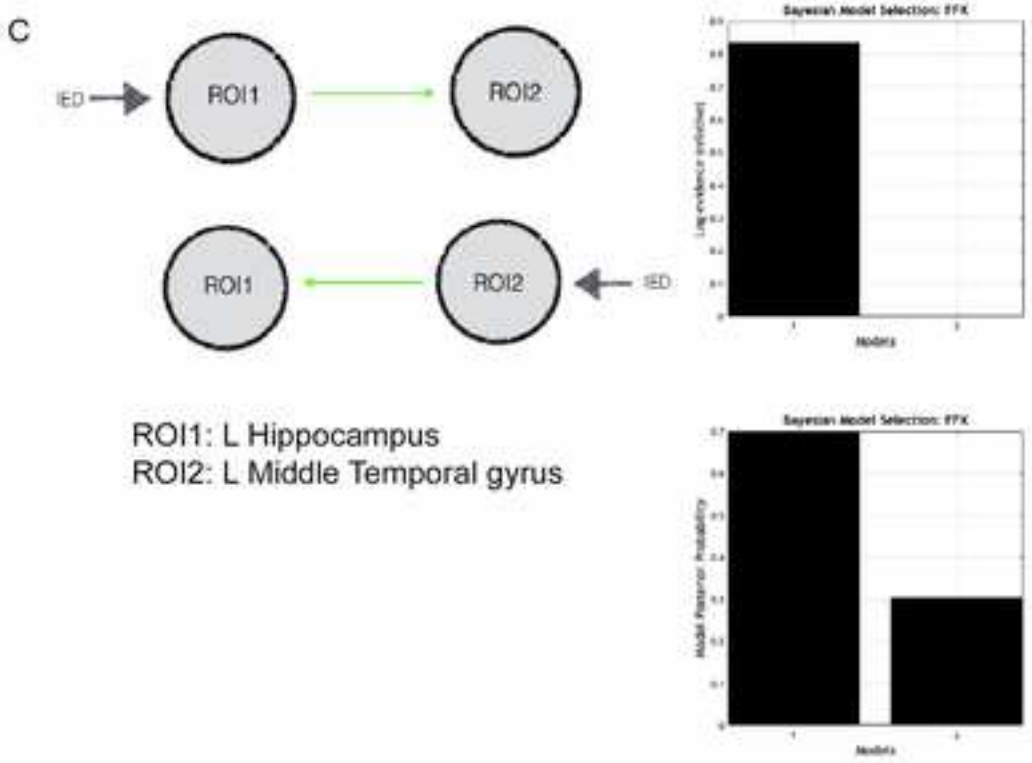

ROI1: L Hippocampus
ROI2: L Middle Temporal gyrus

Figure 4

Table 1

Table 1: Clinical details of patients studied with DCM based on fMRI

Pt ID	Ictal Semiology	Interictal EEG (maximum spike distribution)	Ictal EEG (region of seizures onset)	sMRI	FDG-PET	AED/ daily dose(mg)	icEEG	Epilepsy Surgery	Pathology*	Outcome**/ Follow up (mo) post- surgery
1	Subjective internal tremor, loss of contact, left hand automatic gestural activity; hypermotor activity in sleep	F3; C3	F3	L Medial Frontal FCD	-	DPA/1000 LEV/1000	-	-	-	-
2	(a) Change of facial expression, staring paled, gestural bilateral purposefulness automatisms. Brief confusion afterwards; (b) sudden loss of consciousness, fall and GTC evolution	T4; T6	T6, P4	Negative	R TO and TP hypo	LEV/1500 OXC/1200	R TP and T insular, T1 and T2, TO junction implantation focus temporo-basal and temporal-occipital.	R TO corticectomy plus ATL	gliosis	IA/29
3	Left arm ascending paraesthesia followed by left side mouth deviation and ideomotor slowdown.	F8; T4; T6; diffuse over the right leads	Diffuse with right prevalence	R parietal perisylvian polymicrogyria	No hypo	LCS/400 LTG/150 PER/8	R P implantation revealed a focus P operculum, supramarginal gyrus, inferior parietal lobuli	R P opercolum, R supramarginal corticectomy	gliosis	IA/16
4	Subjective descending-ascending shiver sensation from the head to the stomach, loss of contact, smiling and oral automatisms. Postictal aphasia	F7; T3	--	L mesial temporal FCD	-	PB/75 PRB/225	-	L ATL	FCD IIa	IA/72
5	Subjective vertigo, visual field restriction and oscillation; rare loss of consciousness	F8; T4 T4; T6	T6, O2	R temporo-occipital cortex FCD; R parahippocampal gyrus FCD	-	CBZ/600 CLB/10	-	-	-	-

6	(a)Sleep events: scream, face redness, bilateral clonic arms movements, vocalization; (b)awake, brief epigastric subjective sensation followed by transitory loss of contact	F7; T3	F3, T3	L insular dermoid cyst	-	PRP/6 LTG/200 PB/100	-	-	-	-
7	Right foot paresthesia, tremor with spread to the homolateral shoulder followed by stiffening of the right leg and fall to the floor	Cz; C3; P3	Cz, C3, P3	L Superior Parietal FCD	-	OXC/1500 CLB/10	-	Lesionectomy	FCD IIb	III/24
8	Right visual elementary hallucinations, cephalalgia, right superior arm stiffness, stereotyped vocalizations and dizziness	P3; Pz; T5; diffuse	P3, Pz	L precuneus FCD	L precuneus hypo	LCS/400 PRP/6 LEV200	-	Lesionectomy	FCD I	IIA/24
9	Subjective muffled sound sensation, staring and oral automatisms, ideomotor slowdown	F7; T3	T3	L parahaippocampal DNET	-	CBZ/800	-	-		-
10	Subjective ascending warmth sensation and visual attraction towards surrounding stimuli, foul language, fixed gaze, facial flushing with loss of contact and brief post-ictal confusion	C4; P4	T4, T6, O2	R temporo-occipital AVM	-	CBZ/800	-	Lesionectomy	AVM	III/36

Legend Table 1: (*) Pathology was defined according to Blumcke et al. 2017; (**) Outcome was defined according to the Engel Epilepsy Surgery Outcome Scale; L: Left; R: Right; mo: months; FCD: Focal Cortical Dysplasia; Hypo: Hypometabolism; CBZ: Carbamazepine; LCS: Lacosamide; PRP: Perampanel; LEV: Levetiracetam; OXC: Oxcarbazepine; CLB: Clobazam; LTG: Lamotrigine; VPA: Valproic Acid; PB: Phenobarbital; PRB: Pregabalin; TO: Temporo-Occipital; TP: Temporo-Parietal; P: Parietal; T: Temporal; ATL: Anterior Temporal Lobectomy; GCT:

generalized tonic-clonic evolution; AVM: arteriovenous malformation; FCD: Focal Cortical Dysplasia; DNET: Dysembryoplastic neuroepithelial tumors; sMRI: Structural MRI; FDG-PET: Fluorodeoxyglucose PET.

Table 2

Table 2: EEG-fMRI and DCM results

Pt ID	*IED location / number (type)*	*Presumed EZ/ EEG-fMRI concordance*	*Cluster 1*		*Cluster 2*		*Cluster 3*		*Cluster 4*		*DCM results*	*Independent Validation*
			Localization	*Z score*	*Localization*	*Z score*	*Localization*	*Z score*	*Localization*	*Z score*		
1	F3, C3/106 (S) F3, C3/28(SW)	L Medial Frontal FCD /C+	L Superior Frontal gyrus*	7.45	L Caudal middle Frontal gyrus	6.75	-	-	-	-	Concordant	-
2	T6/98 (SW)	R temporal lateral and basal cortex (T2, TO junction)/ D+	R Middle Temporal gyrus	6.67	R Middle Frontal gyrus	5.55	R Posterior Cingulate gyrus	5.60	R Superior Temporal sulcus	5.45	Concordant	Valid (SEEG & surgery) Confirmed
3	Right fronto-temporal/14 (SW)	Right polymicrogyria (post-central and parietal opercolum)/ D+	L Postcentral gyrus*	5.96	R Postcentral gyrus	5.94	R Enthorinal cortex	5.15	-	-	Concordant	Valid (SEEG & surgery) Confirmed
4**	F7, T3/19 (S)	L mesial temporal FCD/C+	L Anterior Insular cortex*	3.32	L Temporal pole	3.16	-	-	-	-	Concordant	Valid (surgery) Confirmed
5	T4, T6/33 (SW)	R temporo-occipital cortex FCD/D+	R Inferior Parietal Cortex*	5.36	R Fusiform gyrus	4.91	-	-	-	-	Concordant	-
6	F7, T3/204 (S)	L frontal opercolum/C+	L Pars triangularis*	7.39	L Anterior cingulate	6.05	-	-	-	-	Concordant	-
7	F3, C3/918 (S)	L Superior Parietal FCD/D+	L Postcentral gyrus*	4.93	L Paracentral gyrus	3.55	R Postcentral gyrus	3.68	-	-	Discordant	Invalid, (surgery) Unconfirmed
8	T3, PZ C3, P3/43 (SW)	L precuneus FCD/D+	R Superior Parietal cortex*	4.19	L Precuneus	3.26	-	-	-	-	Concordant	Valid (surgery) Confirmed
9**	F7, T3/28 (S)	L parahaippocampal DNET/C+	L Parahippocampal gyrus*	3.60	L Superior Temporal gyrus	3.34	-	-	-		Not Conclusive	-
10	C4, P4/17 (S)	R temporo-occipital MAV/D+	R Superior Temporal gyrus*	5.75	R Middle Temporal gyrus	4.59	R Cuneus	5.16	R Frontal Opercolum	5.41	Discordant	Invalid (surgery) Unconfirmed

Legend Table 2: (*) Global maxima; (**): $p < 0.01$ uncorrected; small volume correction $p < 0.05$ FWE corrected. L: Left; R: Right; SW: spike-wave; S: Spikes.